Late Holocene climate variability and fire history from Deepwater Lake sediments, Fraser Island, South Queensland

Thesis submitted in accordance with the requirements of the University of Adelaide for an Honours Degree in Geology

Mathew Alexander Raven

November 2017

THE UNIVERSITY of ADELAIDE

LATE HOLOCENE CLIMATE VARIABILITY AND FIRE HISTORY FROM DEEPWATER LAKE SEDIMENTS, FRASER ISLAND, SOUTH QUEENSLAND

RUNNING TITLE: CLIMATE AND FIRE HISTORY OF FRASER ISLAND

ABSTRACT

Lake sediments are an important resource that can be used to reconstruct past climate and environmental conditions from all over the world. Understanding past climate changes is extremely important to help understand what's happening to climate in Australia today and potentially into the future. The perched lake systems on Fraser Island in subtropical Queensland, Australia, act as natural rainfall gauges, allowing them to be highly sensitive to environmental changes which, through a variety of indicators, are recorded in the sediments.

Deepwater Lake, a small perched lake on Fraser Island, was investigated using a range of environmental proxies. A detailed chronology was created using a range of accelerator mass spectrometry radiocarbon dates and ^{210}Pb dates on cores taken to a depth of 4.7 m. The chronology indicates an age range of 4800 cal BP to present.

The lake sediments were analysed for carbon isotope ratios, carbon/nitrogen ratio variation, macro-charcoal changes, sediment organic content, magnetic susceptibility, XRF based element geochemistry, ^{210}Pb, and radiocarbon dating. These proxies are used to reflect the changes of catchment processes within the lake environment over the mid to late-Holocene.

The proxies reflect a transition from a dry, fire-prone environment, with very low organic content from 4800-3800 cal BP, to a more rainfall-erosional based environment from 3800-300 cal BP. During the period from 3800-3000 cal BP, it was determined there was a high influx of detrital sediments, organic content, and a transition from an algal based source to a more terrestrial based organic source. Environmental conditions have remained consistent from 3000 cal BP to present day with very little variation observed in the proxies indicating a stabilisation of climate into the late Holocene.

KEYWORDS

Late Holocene, Deepwater Lake, charcoal, palaeolimnology, climate variability, climate reconstruction, fire history

TABLE OF CONTENTS

LIST OF FIGURES

LIST OF TABLES

1. INTRODUCTION

Knowledge about past climate conditions is important in order to understand recent climatic changes, and to create reliable models for future projections of climate change (Snyder, 2010). Lake sediments can provide detailed, centennial-scale records of past climate, as reflected by changes in climate proxies such as charcoal accumulation, elemental abundances and carbon isotopes. In the transition zone between northern tropical Australia and southern temperate areas in particular, there is a lack of detailed climate records, especially over the mid to late-Holocene, (Donders et al., 2006). The perched lakes on Fraser Island provide an opportunity to bridge the gap and create detailed multi-proxy reconstructions of paleoclimate and paleoenvironmental change.

Rainfall variability in eastern Australia has been shown to be predominantly controlled by the strength and variance of the El Niño-Southern Oscillation (ENSO) (Risbey et al., 2009). Multi-year drought events in south-eastern Australia have also been shown to be predominantly driven by the Indian Ocean Dipole (IOD) (Ummenhofer et al., 2009). The periods of highest rainfall occur between November and April, coinciding with the months when the Australian rainfall/ENSO relationship is the most significant (B. F. Murphy and Timbal, 2008; Risbey et al., 2009). The variability in frequency and strength of ENSO events, and their relationship to climate, both past and future, are poorly understood (Tudhope et al., 1995; Zhengyu, 2012). With the help of paleoclimatological data, the behaviour of the ENSO over time can be better understood (Emile-Geay et al., 2013).

In part, as a result of inter-annual rainfall variability, Australia is one of the most fire-prone areas in the world (A. A. J. Williams et al., 2001). Australia's fire regimes range from high intensity and low frequency in the temperate south of Australia to low intensity and high frequency fires in the northern savannas (Russell-Smith et al., 2007; A. A. J. Williams et al., 2001). Charcoal analysis has been used on Fraser Island to indicate that periods of increased fire occurrences correlates with periods of drier vegetation and low lake levels (Donders et al., 2006). Short term reconstructions of fire regimes and vegetation systems that focus on the Holocene in eastern Australia are rare (Barr et al., 2013; Black et al., 2006). Therefore contiguous charcoal records are important in constraining the prediction of past and future fire regimes.

There have been few investigations into past climate focused on Fraser Island. Donders et al. (2006) looked at vegetation dynamics and forest succession at Lake Allom to indicate past temperature conditions. Woltering et al. (2014) attempted to reconstruct temperature variability from 37 ka cal BP using branched glycerol dialkyl glycerol tetraether (*b*GDGT) distributions from Lake McKenzie. Atahan et al. (2015) used pollen and stable isotopes from Lake McKenzie for evidence of late Quaternary environmental change. Hembrow et al. (2014) also looked at diatoms within a Lake McKenzie core to investigate interactions between climate influences and aquatic ecosystems. Longmore (1997b) studied Hidden Lake, using assorted techniques to constrain changes in vegetation and climate over the Holocene. Much of the understanding of Holocene climate in eastern Australia is sourced from only a few sites from Fraser Island, North Stradbroke Island and coastal Australia. This study aims contributes to this understanding in a substantial way with an additional, detailed, late-Holocene climate record.

The aim of this thesis is to present a record of the past 5000 years of climate variability on Fraser Island, Queensland, created from a multiple proxy approach to climate reconstruction. Indicators used include basic sediment analysis, carbon isotope ratios, C/N ratios, macro-charcoal analysis and XRF core scanning. An age-depth model for the sediment core is created using a combination of ^{210}Pb dating and radiocarbon dating. Comparison between current long term climate models such as the well documented ENSO, specifically in the Southern Hemisphere, will help develop a greater understanding of the ecological and environmental processes occurring within Australia over the mid- to late-Holocene.

2. BACKGROUND AND SITE DESCRIPTION

Fraser Island is the world's largest sand island, located off the east coast of subtropical south-eastern Queensland (Figure 1). The landmass of Fraser Island is composed of Quaternary sand dunes that were formed during periods of low sea level (Lees, 2006). There are nine parabolic dune systems which reach a maximum height of 250 m above sea level (Longmore, 1997a).

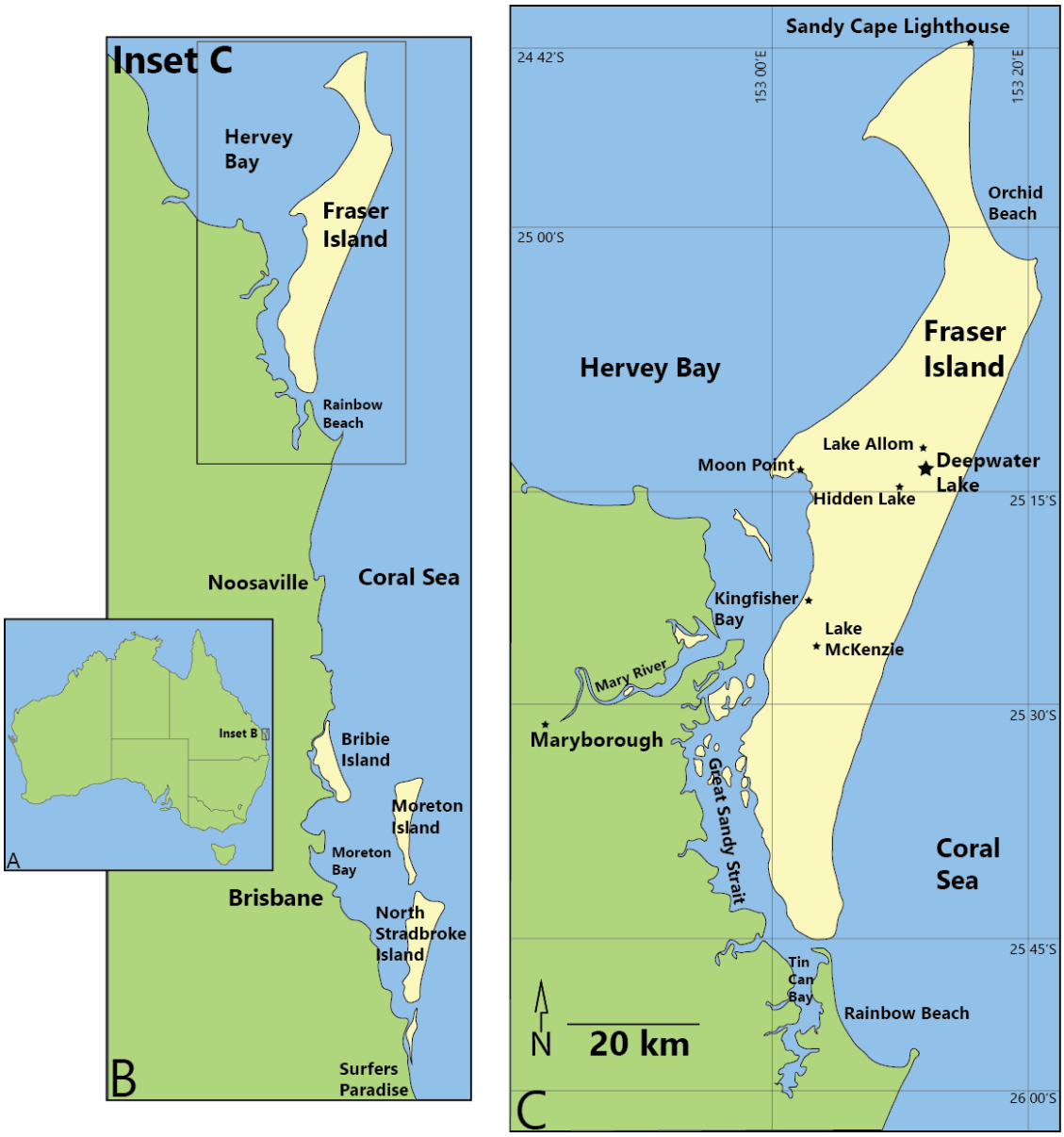

Figure 1: Map showing location of Fraser Island, East of Maryborough in south eastern Queensland. 1a) Australia. 1b) South eastern Queensland. 1c) Fraser Island, Positions of previously studied Lake McKenzie (Hembrow et al., 2014; Woltering et al., 2014), Lake Allom (Donders et al., 2006), Hidden Lake (Longmore, 1997a) and the current study site of Deepwater Lake are indicated. Map adapted from (Gontz et al., 2015).

Fraser Island contains many perched lakes filled with highly organic-rich sediments. These perched lakes have formed due to an impermeable base-layer (B-horizon) of sediment, termed “coffee rock”, that has formed beneath these lakes where organic matter has accumulated over time and been cemented with a sandy substrate (Timms, 1986). The isolation of the perched lakes from the water table, along with the B-horizon, prevent water from percolating in and out of the bottom of the lakes.

Deepwater Lake (DWL) is a narrow perched lake located in central Fraser Island. At the time of sediment coring, the lake was 4.9 m deep. The lake is located 63 m above sea level, with a surface area of approximately 150 m^2 as of 2017 (Google Maps, 2017). DWL has a steep catchment reaching up to 100 m above sea level on both the north-east and south-west fringes of the lake. The lack of continuous inflow and outflow creeks connected to DWL allow the lake level to be highly responsive to changes in evaporation and precipitation rates, making it perfect for paleoclimate reconstruction. These conditions are similar to those investigated at Lake McKenzie (Atahan et al., 2015), although DWL is a much smaller lake, and therefore potentially much more responsive to past climate and environmental changes.

The flora of Fraser Island is dominated by a mixture of woodland, dry sclerophyll, rainforest, and heath communities. During dry conditions sclerophyll forests are often dominated by a short grassy understory, where fires are often of low intensity and infrequent (B. P. Murphy et al., 2013). In periods of higher rainfall, sclerophyll forests are dominated by a shrub understory, where fires can reach a higher intensity (Bradstock, 2010; B. P. Murphy et al., 2013). The vegetation surrounding Deepwater Lake is dominated by tall open to closed dry sclerophyll forests.

Fraser Island has a subtropical climate with light to strong south-easterly prevailing winds, which often bring rain to the island. On occasion, tropical cyclones from the north, bring substantial rainfall from December to April (Lourensz, 1981). The rainfall variability on Fraser Island is strongly influenced by the ENSO, the driver of short-term variability in climate in south-east Queensland (B. F. Murphy and Ribbe, 2004). The majority of rainfall on Fraser Island occurs during the summer to early autumn months from December to April. The average mean annual rainfall at Sandy Cape Lighthouse on the northern tip of Fraser Island is 1250 mm (Figure 2).

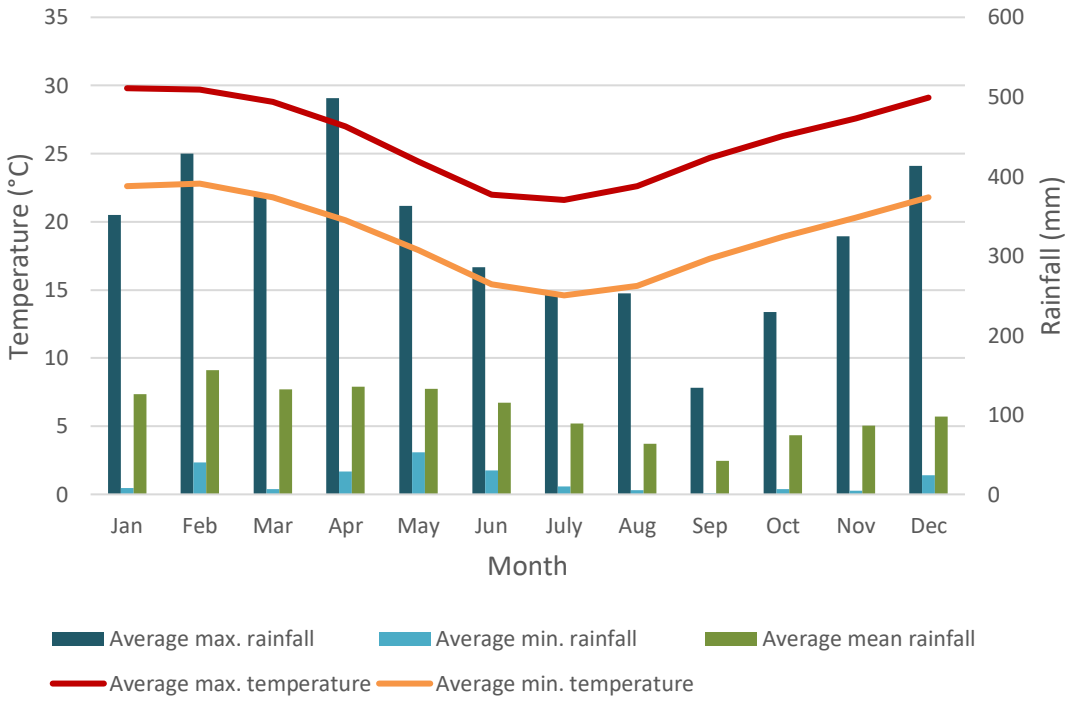

Figure 2: Climate data from Sandy Cape Lighthouse on the northern tip of Fraser Island (Figure 1). Showing average rainfall and temperature over the period from 1981-2010. Data sourced from the Australian Bureau of Meteorology (2017). Climate data showing averages from 1981-2010 (BOM, 2017).

The sediments of Fraser Island's perched lakes are mainly composed of allochthonous organic material, which has been washed or blown into the lakes, and clumps together into organic colloids over time (Longmore and Heijnis, 1999). In addition to the organic

lake mud, the perched lakes can also contain siliceous inorganic sediments and material washed or blown in from the lake catchments or from further afield (Longmore, 1997b).

The lakes on Fraser Island have been the focus of a small number previous studies, but none specifically examining Deepwater Lake. Longmore (1997a) examined Hidden Lake (Figure 1C), inferring a mid-Holocene dry period, from 8.5 ka to 2.5 ka, with the use of vegetation dynamics and climate proxies. This dry period appears to have occurred in anti-phase, with moist mid-Holocene periods from south-eastern Australia (Longmore and Heijnis, 1999). Evidence from pollen and charcoal analysis of sediment from Lake Allom (Figure 1C) indicate a transition from dry conditions in the early Holocene to high lake levels and increasing forests between 5.5 and 3 ka cal BP. An additional diversification towards present day sub-tropical rainforest vegetation occurs from 3-2 ka cal BP (Donders et al., 2006). A sediment core from Lake McKenzie (Figure 1C), was analysed by Woltering et al. (2014), using branched glycerol dialkyl glycerol tetraether (*b*GDGT) distributions to reconstruct mean annual air temperature from between 37 ka cal BP and the present. They found lower average temperatures from between 5.2 and 2.9 ka.cal BP Changes in the lake ecosystem and surrounding vegetation has also been analysed by Atahan et al. (2015), using multiple methods including the use of stable isotopes, macro-charcoal, biomarkers, and pollen. Atahan et al. (2015) found subtle reduction in moisture commencing around 6.1 ka cal BP lasting until around 2.5 ka cal BP, indicating dryer conditions in the mid-Holocene. Hembrow et al. (2014) shows that an increase in $\delta^{15}N$ values between 8 and 4 ka cal BP suggests a wetter phase with an increase in lake depth and primary productivity. While the overall trend of decreasing C/N ratio indicates shallower lake conditions and a potential

reduction of terrestrial organic matter entering the lake due to a decreasing effective precipitation.

Reconstructed lake levels from two hydrologically closed maar crater lakes in south-eastern Victoria have shown declines in lake levels starting from 7.2 ka to minimum levels between 1.8 and 1.3 ka (Wilkins et al., 2013). The inconsistencies with climate reconstructions over the Holocene suggests that there are potentially local factors that are having important influences on the climate of Fraser Island.

3. METHODS

3.1 CORE COLLECTION AND DESCRIPTION

In 2016, an extruded sediment section and two full sediment cores were collected from Deepwater Lake from a water depth of 4.7 m. The first 123 cm of sediment (extruded core) was collected using a soft sediment piston corer, which extrudes sediment vertically, in discrete 1 cm increments. The core sections were stored in bags until the sediment was consistent enough to maintain shape and lithology. Two full sediment cores were taken from the centre of DWL using a Bolivia piston corer (Wright Jr, 1967). The first core (16/01) covers a depth from 0 m to 5 m, the second core (16/02) was offset 0.5 m giving a depth of 0.5 m to 5 m. The cores were extracted in five 1 m drives, sealed in the field, transported to the laboratory and stored in a cold room at 4°C until required for analysis.

The cores were opened lengthways using a reciprocating saw and knife, before being sliced in half by pushing a metal sheet through the cuts. Both of the cores underwent continuous sediment description and digital photography (Appendix A). This project

focuses on the extruded core and the first four drives of the second core (16/02 0.5-4.5 m).

3.2 Core correlation

Since the ITRAX data comprehensively shows element abundances within the sediment, it was possible to identify an overlap between the extruded core (0-123 cm) and the main DWL core. Connections between the sediment records of both cores are expressed in data series as peaks or troughs which occur in overlapping series. Both magnetic susceptibility (Verosub and Roberts, 1995) gained from the ITRAX scanner, and Fe/cps were plotted on a single graph and obvious peaks and troughs were correlated.

3.3 Loss on Ignition

Sediment moisture content was determined from the mass lost following overnight drying at 105°C. Weight lost on ignition of the samples at 550°C for 4 hours was used to determined organic content. Loss on Ignition (LOI) was performed on contiguous 1 cm intervals, with ½ cm^3 of sediment used for combustion (Heiri et al., 2001). Organic content for the extruded core was inferred from the ratio of incoherent to coherent (Inc/Coh) scattered X-rays from the ITRAX Core scanner (Gadd, 2016).

3.4 Geochronology

To provide age estimates of the extruded core, six ^{210}Pb dates and one radiocarbon date were determined. For the remainder of the main core, five radiocarbon dates were determined. Evenly spaced sub-samples of the main core were taken for conventional radiocarbon analysis. The samples of lake sediment, leaf, and stick fragments, were

analysed using accelerated mass spectrometry (AMS) ^{14}C dating at the Australian Nuclear Science and Technology Organisation (ANSTO) STAR accelerator facility (Fink et al., 2004). Radiocarbon ages were calibrated with the use of the Southern Hemisphere data set (Hogg et al., 2016) in Bacon (Blaauw and Christen, 2011) and are shown as the median probability of the two sigma distribution of calendar ages. The calibrated ages are shown as years before 1950 (cal yr BP).

The ^{210}Pb dates were sampled from the first 18 cm of sediment in the extruded portion of the core. Measurements were made using alpha spectrometry at the ANSTO facility (Fink et al., 2004), and are shown as both calculated constant initial concentration (CIC) ages and calculated constant rate of ^{210}Pb supply (CRS) ages (Appleby, 2001).

An age-depth model was developed using the Bacon program (Blaauw and Christen, 2011) (version 2.2) in R (Team, 2017).

3.5 Charcoal analysis

Additional 1 cm^3 sub-samples of sediment were taken at contiguous 1 cm intervals, and prepared for charcoal analysis following an adapted method of organic matter removal by hydrogen peroxide (H_2O_2) digestion (Mooney and Radford, 2001). A solution of 10% H_2O_2 was mixed with the sediment and agitated twice over a 3-5 day period to decolour and remove organic matter, before being wet sieved through nested sieves of sizes 250 μm and 125 μm, using the method described by Long et al. (1998). Charcoal size fractions of >125 μm were chosen because they are rarely found outside a 10 km radius of a recent fire (Long et al., 1998; Millspaugh and Whitlock, 1995).

Both size fractions were individually dispersed in separate petri dishes and photographed using a Canon EOS 40D digital camera with a 100 mm macro lens and flash (Figure 3A). Images were converted in Adobe Photoshop (Version 13.0) to the

correct file size, and a 50% higher contrast and brightness setting applied (Figure 3B), before analysis with ImageJ (Schindelin et al., 2015). The colour channels were split into blue, green and red, with both blue and green discarded (Figure 3C). The threshold was adjusted to highlight the charcoal particles in the red channel before charcoal count, charcoal area and average charcoal size, was recorded by ImageJ (Figure 3D). (Mooney and Black, 2003). Charcoal particles are expressed as particles per gram of sediment (particles/g). Charcoal area is expressed as mm^2 per gram of sediment (mm^2g^{-1}).

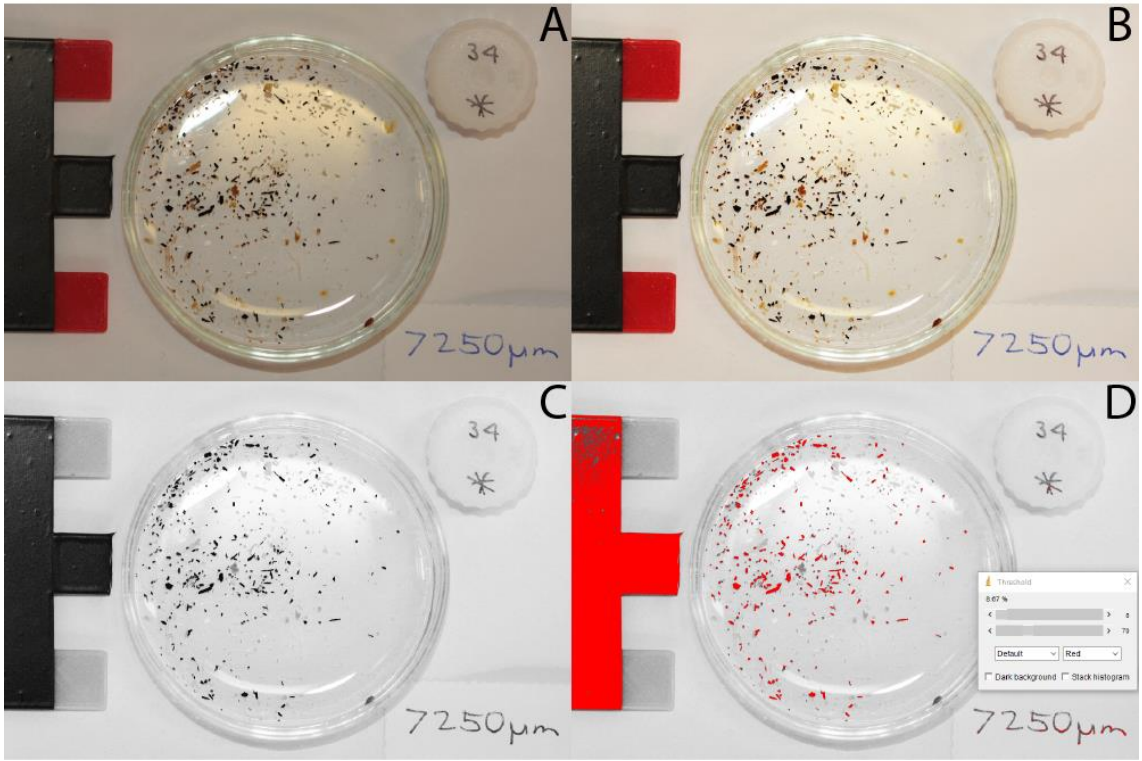

Figure 3: Charcoal images outlining method. 3a) Raw image of sieved charcoal fraction >250 µm dispersed in a petri dish 3b) Charcoal image after conversion in Photoshop to 50% higher contrast and brightness. 3c) The red channel charcoal image shown after removing the blue and green channels, indicating charcoal fragments as black. 3d) Charcoal image following increasing of threshold to 70. Charcoal fragments appear red.

3.6 Carbon isotopes and C/N ratio analysis

Approximately 1 g of sediment (1 cm^3) was extracted at 9 cm intervals, with additional samples used from the bottom 74 cm due to increased visible stratigraphy. The samples were analysed at the NERC Isotope Geosciences Laboratory (NIGL) at the British

Geological Survey (BGS). Standard methods for acid pre-treatment were used to prepare samples for carbon/nitrogen isotope analysis (P.A Meyers and Teranes, 2001). The samples were acidified with 50 ml of 5% HCl to remove carbonates. The acid treated fraction was decanted and washed with de-ionised water until a neutral pH was reached. The remaining sample was dried overnight at 40°C, and gently ground to a fine powder.

Carbon isotope analysis, ^{13}C and ^{12}C, was performed by combustion in a Costech Elemental Analyser on-line with a VG TripleTrap and Optima dual-inlet mass spectrometer. Calculated $\delta^{13}C$ values were determined to the Vienna Pee Dee Belemnite (VPDB) scale, using within-run laboratory standards calibrated against NBS18, NBS-19 and NBS-22. Replicate analysis of well-mixed samples indicated a precision of + <0.1‰ (1 SD). C/N ratios were calibrated against an Acetanilide standard. The resulting data includes %N, %C, C/N ratio and $\delta^{13}C$ results.

3.7 XRF geochemical analysis and magnetic susceptibility

The full sediment core from DWL, including the discrete samples from the extruded core and a U-channel from the remaining extruded core (19-123 cm) were sent to the ANSTO facility (Fink et al., 2004), and underwent non-destructive, high-resolution XRF scanning to record element abundances in the sediment. The instrument used was an ITRAX XRF core scanner from Cox Analytical. The core was scanned at 1000 μm step intervals, with a count time of 10 seconds per increment, using a Cr tube operating at 2200 W. The individual element spectra were deconvolved in real time during the scanning to construct profiles of peak element abundances (Appendix B). The first 19 cm of the extruded core were analysed as discrete samples under the scanner, and so

the resulting data was averaged and stitched together to create a full record. Optical (Figure 4) and radiograph images (not shown) were also taken along the extruded core from both 19-123 cm and the full length of the main core (Figure 4). Magnetic susceptibility readings were also taken at 5000 micron increments from 19-123 cm of the extruded core and the full length of the main core.

During the XRF scanning process of the cores, the breaks between individual drives was noted and was manually removed using a combination of counts per second (CPS) for readings below 25,000, and mean standard errors (MSE) for readings above 2.5. The ITRAX data values are presented as CPS.

4. RESULTS

4.1 Core description

At the very base of the core, there is a thick, fibrous plant mat. From 460-455 cm there is a coarse grained sandy layer. From 455-450 cm, there is a layer of dark organic matter, with large amounts of charcoal visible. From 450-408 cm, the core is dominated by sand, with varying amounts of dark organic matter spread throughout. From 408 to 398 cm, the very dark organic layer returns, before transitioning to dark brown, sandy sediments from 380-370 cm. From 370-361 cm, the amount of organic matter increases and from 361-355 cm, there is a final very dark organic rich layer.

From 355-290 cm there are large amounts of organic matter, leaves, and rootlets, with very little to no visible sand. There is a coarse sand layer from 290-280 cm, before the sand content reduces and transitions to organic matter from 280-255cm.

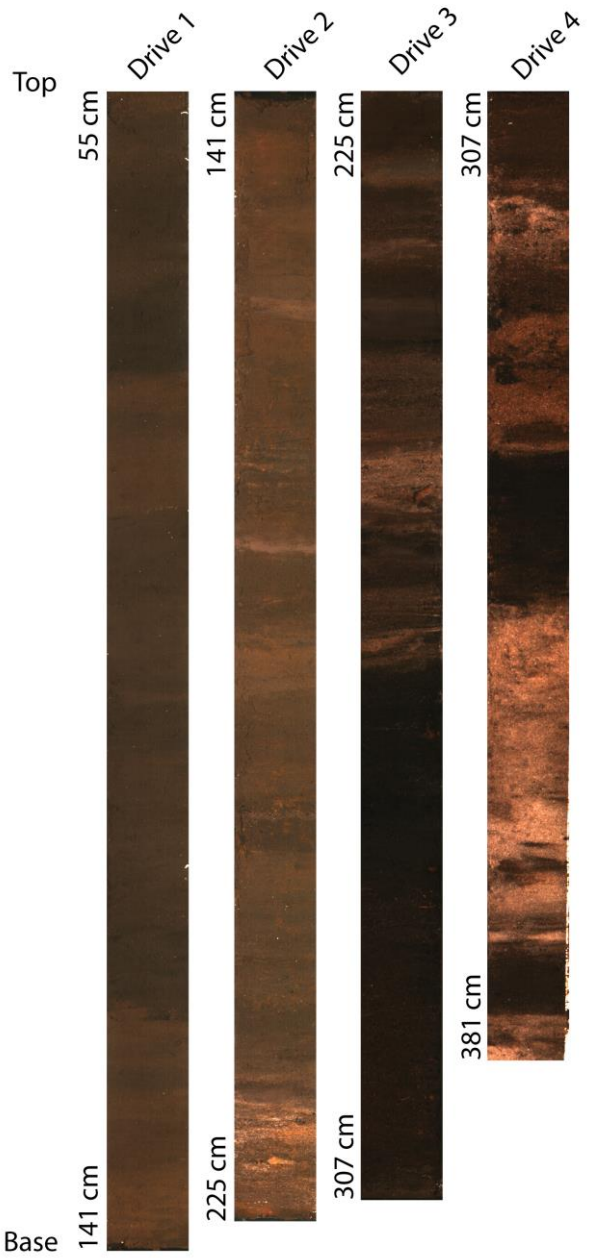

Figure 4: Optical imaging of DWL core drives, obtained from ITRAX core scanning of individual drives. Images have not been corrected for compaction, therefore are shown with the uncorrected depth measurements.

The two remaining drives from 255 cm to 55 cm show almost no visible variation in sediment composition. Both consist of homogenous black-brown organic lake mud, with some small sand grains visible in some sections (Figure 4).

The extruded core portion (0-55 cm) consists of homogenous black-brown organic lake mud, including small amounts of medium to fine grains of sand throughout. There are very little to no visible changes in lithology throughout the first 55 cm of sediment. During ITRAX core scanning of the drives, optical images were captured showing lithological changes (Figure 4).

4.2 Core correlation

The iron counts (cps) and magnetic susceptibility readings from the ITRAX core scanner were used to correlate the two overlapping cores (Appendix C). Agreement between the two proxies allowed the correlation of a single core depth scale, excluding the lower 68 cm of the 123 cm extruded core. This resulting correlation was verified by comparison of radiocarbon dates obtained from both cores. The correlation resulted in a total 0-461 cm full sediment record. All depths used in this study are based on the correlated full core.

4.3 Compaction correction

During the sediment coring process, sediment undergoes slight compaction during the extraction process. To account for this compaction, the amount of sediment recovered in the drives is extrapolated to the actual length of the original drives, and the new depth values are used in the remaining calculations (Table 1).

Table 1: Compaction correction of the DWL sediment drives.

Drive	Core Depth (mm)	Sediment recovered (mm)	Compact correction
Extruded	550	550	1
1	1000	860	1.162
2	1000	840	1.190
3	1000	820	1.219
4	1060	740	1.432

4.4 Loss on Ignition

Sediment sub-samples used for organic matter and moisture estimating using LOI were only taken from the main sediment core (55-461 cm), and not from the extruded section. The high moisture content throughout the core shows strong correlation with organic matter, decreasing proportionally with the decrease in organic matter in the core. Organic content shows seven discrete periods of change within the sediment record, beginning at 4800 cal BP until 4600 cal BP there is some variation between 0% and 20%.

Organic content drops to 0-1% from 4600-4250 cal BP, spiking to 40% from 4250-4100 cal BP, before returning to 0-10% organic content from 4100-3900 cal BP. From 3900-3500 cal BP, the organic content in the core increases to an average of 40%, then decreases to an average of 10% from 3500-3000 cal BP. Organic content then increases to levels between 20% and 30% from 3000-850 cal BP, where organic content in the sediments remains relatively steady (Figure 5).

The organic content of the extruded core was estimated using the ratio of the Inc/Coh data from ITRAX scanning (Figure 5). This is possible because organic carbon has a lower average atomic mass than silica, aluminosilicates, and carbonates. An increase in Inc/Coh ratio therefore suggests a greater organic carbon concentration and higher organic matter content (Burnett et al., 2011). Another method for estimation of organic

content is the total organic carbon (TOC) found in bulk sediment, which is shown to correlate with the LOI values (Figure 5).

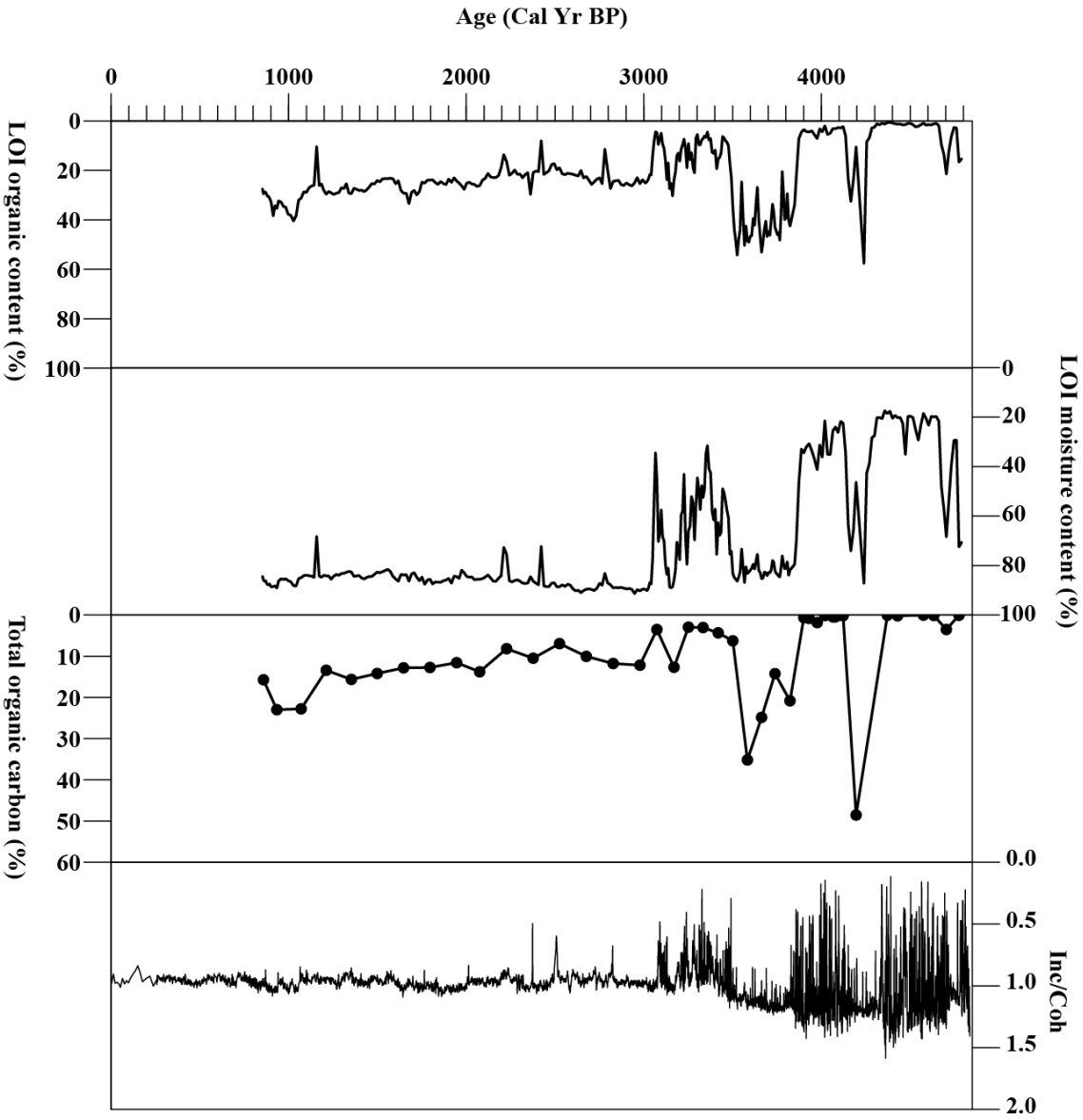

Figure 5: Measures of organic content within DWL core (organic content, moisture content, total organic carbon and Inc/Coh).

4.5 Geochronology

The results of the five radiocarbon dates and six ^{210}Pb dates of sediments taken from DWL are shown in Table 2 and 3, respectively. The radiocarbon sample OZV937 (41-43 cm: sediment) has a calibrated age that is older than sample OZV938 (63.5 cm: leaf).

This difference is likely due to the differing sample types, as bulk organic sediment has a larger possibility of error, due to mixing of carbon sources (e.g. charcoal which can persist in the landscape for long periods of time) than a single leaf sample. The ^{210}Pb sample id: T762 (17-18 cm) has a missing CRS age and an extrapolated CIC age, as there was no excess ^{210}Pb recorded for that sample.

Table 2: Radiocarbon dates and calibrated age ranges for Deepwater Lake core. All possible calibrated age ranges are shown, along with the probability within each age range.

ANSTO ID	Sample Type	Depth (cm)	Conventional Radiocarbon Age	SD	δ13C per mil	Calibrated age range (yrs. BP)	Probability
OZV937	Lake sediment	41-43	1,045	25	-27.2	808 – 868 901 - 959	32.9 67.1
OZV938	Leaf	63.5	875	30	-28.6	682 - 789	100
OZV940	Lake sediment	207.5	3,060	30	-28.4	3077 – 3096 3105 – 3273 3284 - 3342	4.4 75.7 19.9
OZV941	Leaf and other organics	289.5	3,475	30	-30.0	3589 – 3734 3740 – 3778 3787 -3827	77.5 8.9 13.7
OZV942	Stick and other organics	311.5	3,490	30	-29.7	3614 – 3624 3628 - 3830	1.8 98.2

Table 3: ^{210}Pb dates, dry bulk density, total ^{210}Pb, calculated CIC and CRS ages for DWL extruded core. The final calculated CIC age for sample T762 has been calculated by extrapolation of known ages due to undetected ^{210}Pb decay values (shown in red).

ANSTO ID	Depth (cm)	Dry Bulk Density (g/cm^3)	Total ^{210}Pb (Bq/kg)	Supported ^{210}Pb (Bq/kg)	Unsupported ^{210}Pb Decay corrected to 14/08/2017 (Bq/kg)	Calculated CIC Ages (years)	Calculated CRS Ages (years)
T757	1-2	0.09	250 ± 12	15 ± 1	235 ± 12	13 ± 4	13 ± 1
T758	3-4	0.10	178 ± 9	27 ± 2	151 ± 9	31 ± 5	31 ± 3
T759	5-6	0.14	95 ± 4	29 ± 3	66 ± 5	54 ± 5	54 ± 5
T760	9-10	0.13	40 ± 2	26 ± 2	14 ± 3	106 ± 7	100 ± 13
T761	13-14	0.14	32 ± 1	28 ± 2	4 ± 3	157 ± 8	149 ± 29
T762	17-18	0.12	34 ± 1	34 ± 3	Not detected	208 ± 9	-

An age-depth curve (Figure 6C) was constructed following calibration of the measured ^{14}C dates in BACON (Blaauw and Christen, 2011). The dates provide a coherent estimation of sediment age, which increase with increasing depth. An additional date is

included at the top of the core to estimate the age of top surface sediment as it was gathered in 2016. The dates suggest a relatively constant rate of sediment accumulation of approximately 0.1 cm per year and a mean basal age for the core of 4852 calibrated years before present, where present day is 1950 (cal yr BP) (Figure 6B).

All further description of results will be undertaken using the median sediment ages sourced from the Bacon age model (Figure 6C).

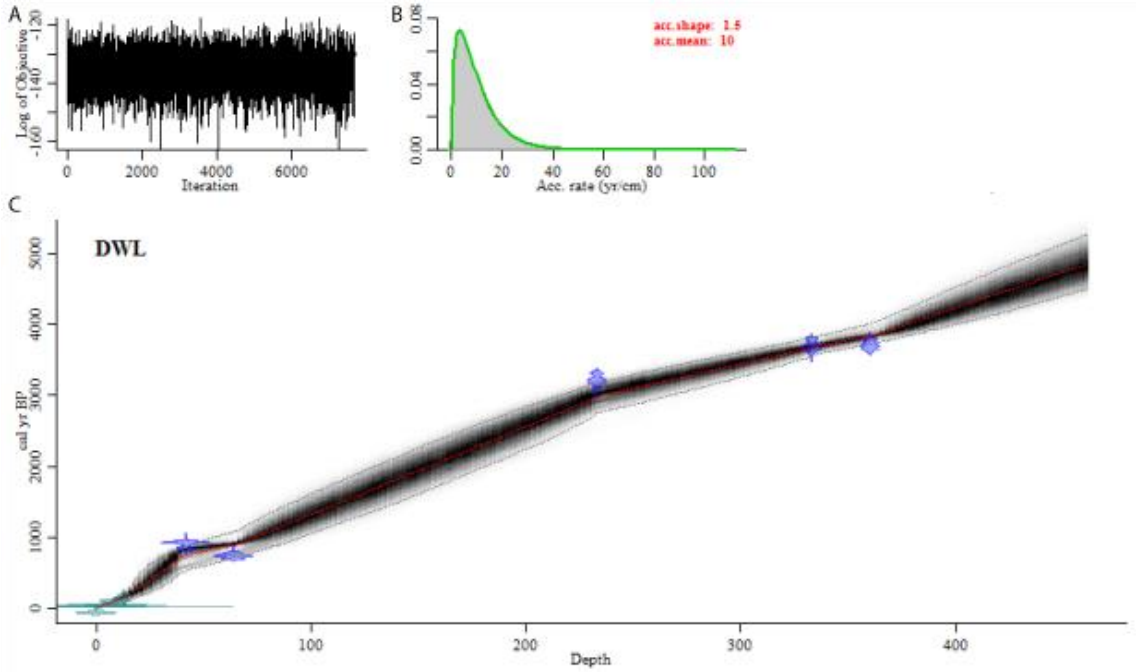

Figure 6: Age vs depth relations for DWL core based on age model information given in table 2 and 3. 6A) the number of iterations for the model. 6B) sediment accumulation rate of the DWL sediments (yr/cm). 6C) the Bayesian age-depth model performed with BACON (Blaauw and Christen, 2011) for Deepwater Lake derived from ^{210}Pb (light blue) and radiocarbon ages (blue) of organic samples taken from DWL core. The solid red line is the weighted averages of all possible chronologies. The uncertainties are represented by the grey shaded area, with 95% confidence intervals outlined by the black dotted lines.

4.6 Charcoal analysis

The oldest sediments in the core are characterised by the highest total charcoal abundances recorded in the sediment record (Figure 7). The charcoal record consists of 195 samples analysed between the base of the core (457 cm) and the top (0 cm). A total

of 85% of the charcoal samples were taken from between 0 and 185 cm, covering a time period of 2400 cal BP.

The charcoal record from 4800-4000 cal BP shows the largest levels of charcoal influx, evident from both particle count (particles/g) and area (mm^2g^{-1}) of charcoal (Figure 7). There are three large peaks within this period: 4700 cal BP, 4200 cal BP and 4050 cal BP, where there are over 200 particles per gram of sediment. From 4000-2100 cal BP, charcoal begins to show a decreasing trend of both amount of particles and charcoal area, before reaching a consistent average amount of charcoal from 2100 cal BP to present time.

The frequency of small peaks in the time period from 2100 cal BP to recent times is due to an increase in resolution of sampling. Due to similar trends in number of particles and charcoal area for both size fractions, the area of charcoal for the >250 μm sized particles was used to represent trends in charcoal for this study.

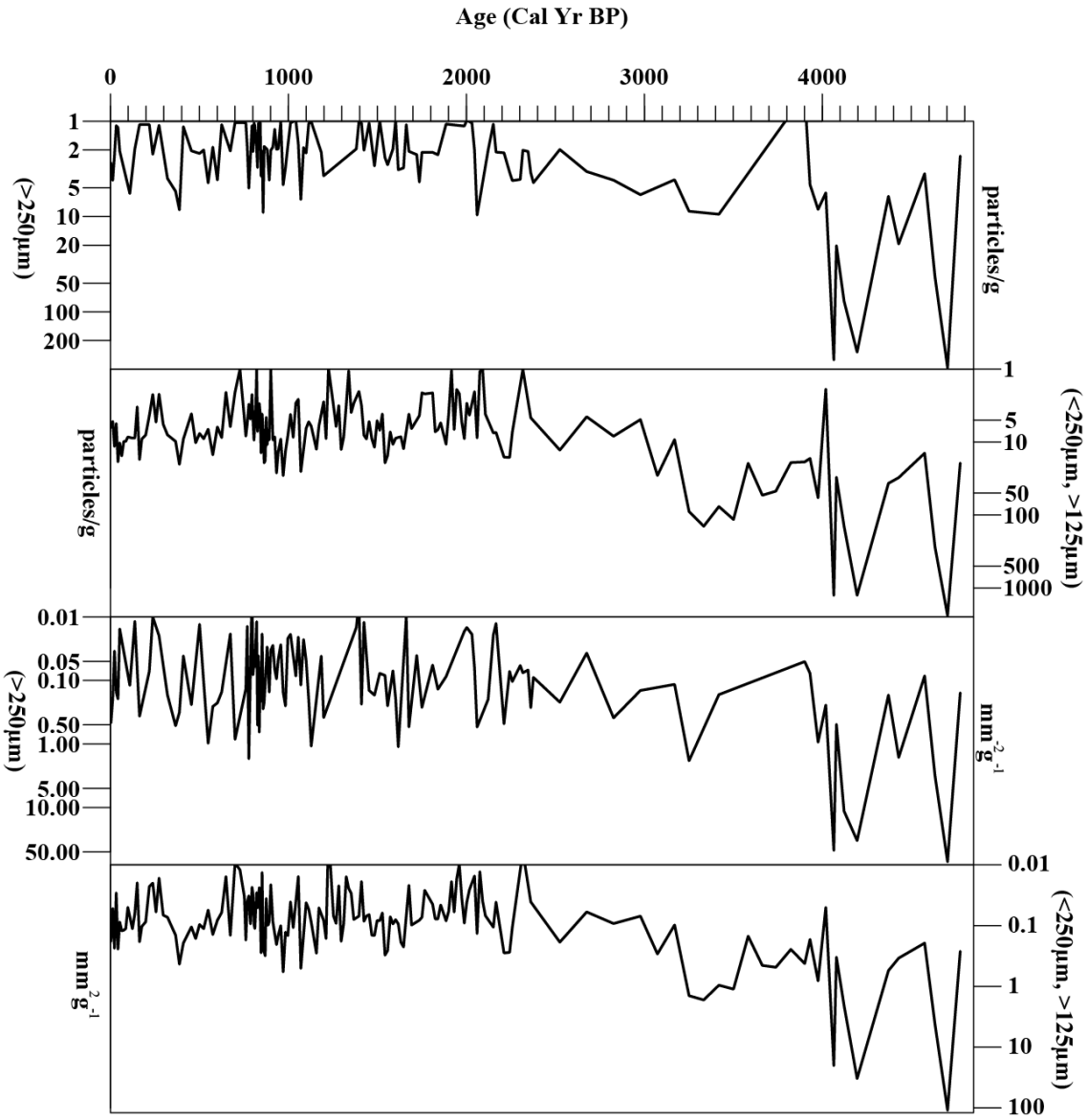

Figure 7: Representation of charcoal particles/g and mm^2g^{-1} in DWL core. Y axis represented in logarithmic scale. Note higher frequency in sampling from 2000-0 cal BP.

4.7 Carbon isotopes and C/N ratio analysis

The percentage of total organic carbon (TOC) values show similar trend as the organic content determined by LOI (Figure 5). This indicates that LOI organic content is a good estimate of TOC in this environment.

From 4800-3800 cal BP, the C/N ratio varies, showing a slight decreasing trend (Figure 8). From 3800-3500 cal BP, the C/N ratio decreases from between 20 and 30, to values less than 10.

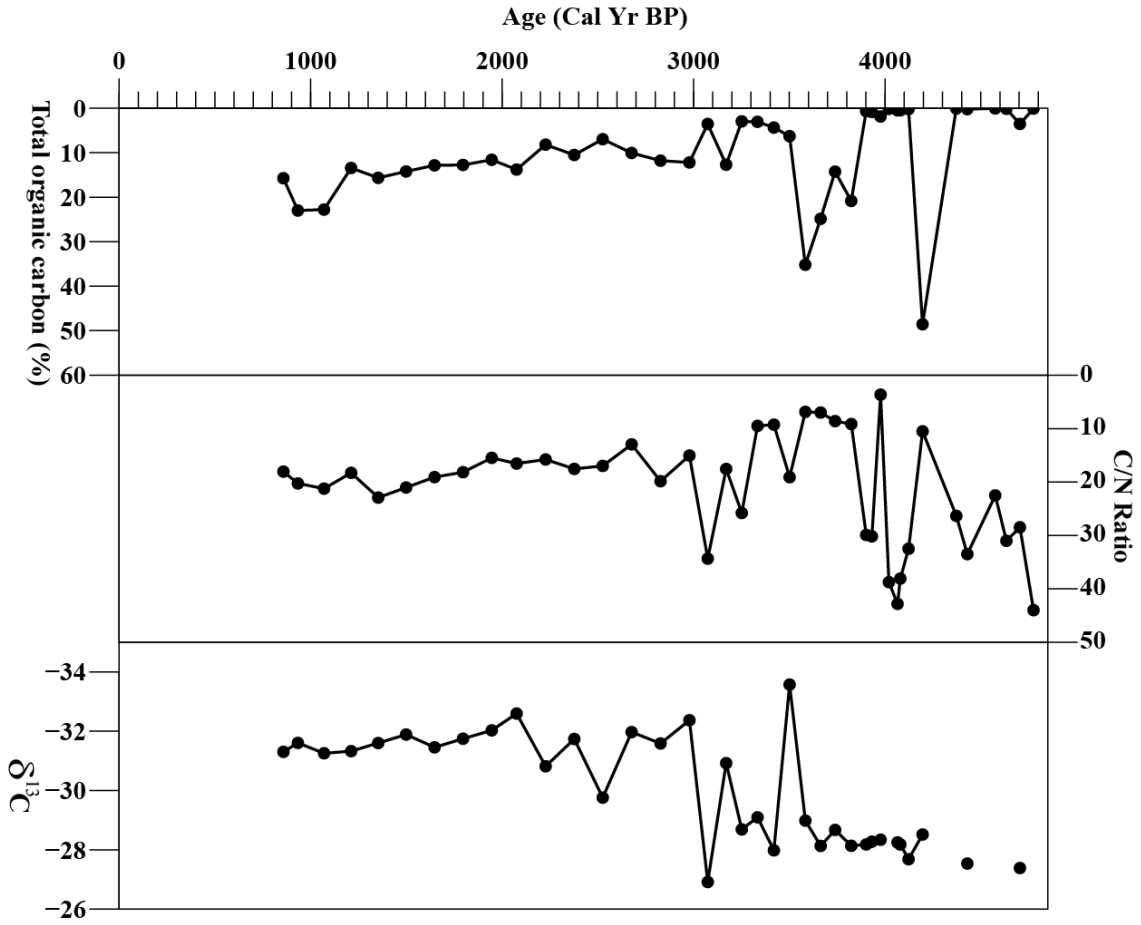

Figure 8: Total organic carbon (TOC), C/N ratio and δ^{13}C of sediment sub-samples taken from DWL.

From 3500-3000 cal BP, C/N ratios show a gradual increase from approximately 10, to a maximum of 40, before stabilising during the 3000-800 cal BP period between 15 and 25. δ^{13}C levels remains constant at approximately -28‰ between 4800-3000 cal BP, with the exception of a single decrease to -33‰ at 3500 cal BP. δ^{13}C then decreases to an average of -32‰ for the remainder of the measured sediment core, 3500-800 cal BP. (Raw Carbon isotope and δ^{13}C presented in Appendix D)

4.8 XRF geochemical analysis

Selected elemental profiles obtained from ITRAX scanning are shown in figures 9 and 10. The elemental profile for Si shows high counts from the beginning of the record (from 4800-4300 cal BP). The Si profile then shows a sharp decline at 4300 cal BP and periods of peak counts from 4100-3800 cal BP and 3500-3100 cal BP. Elemental profiles for Ti and K display similar trends, with both showing large peak periods from 3500-3000 cal BP.

The Ca elemental profile shows consistent values from the beginning of the record (4800 cal BP) until 900 cal BP, where a sharp increase I counts is followed by a period of consistently high values, until 300 cal BP where values begin to decrease towards the end of the record.

The Fe elemental profile only begins to show in the sediment record from 3300 cal BP, and increases steadily through to the end of the sequence (Figure 9). Elemental profiles for Al, S and Br display similar trends throughout the entire record (Figure 10), however S shows several much larger variations at 3300 cal BP and 3200 cal BP in comparison to Al and Br. There are two broader peak periods at 4750 cal BP and from 4200-4300 cal BP before the levels transition to lower values and stabilising throughout the remainder of the record. The elemental profile for Zr displays few minor peaks throughout the record except for a period from 3900-3100 cal BP where there is a large increase in Zr content during this period.

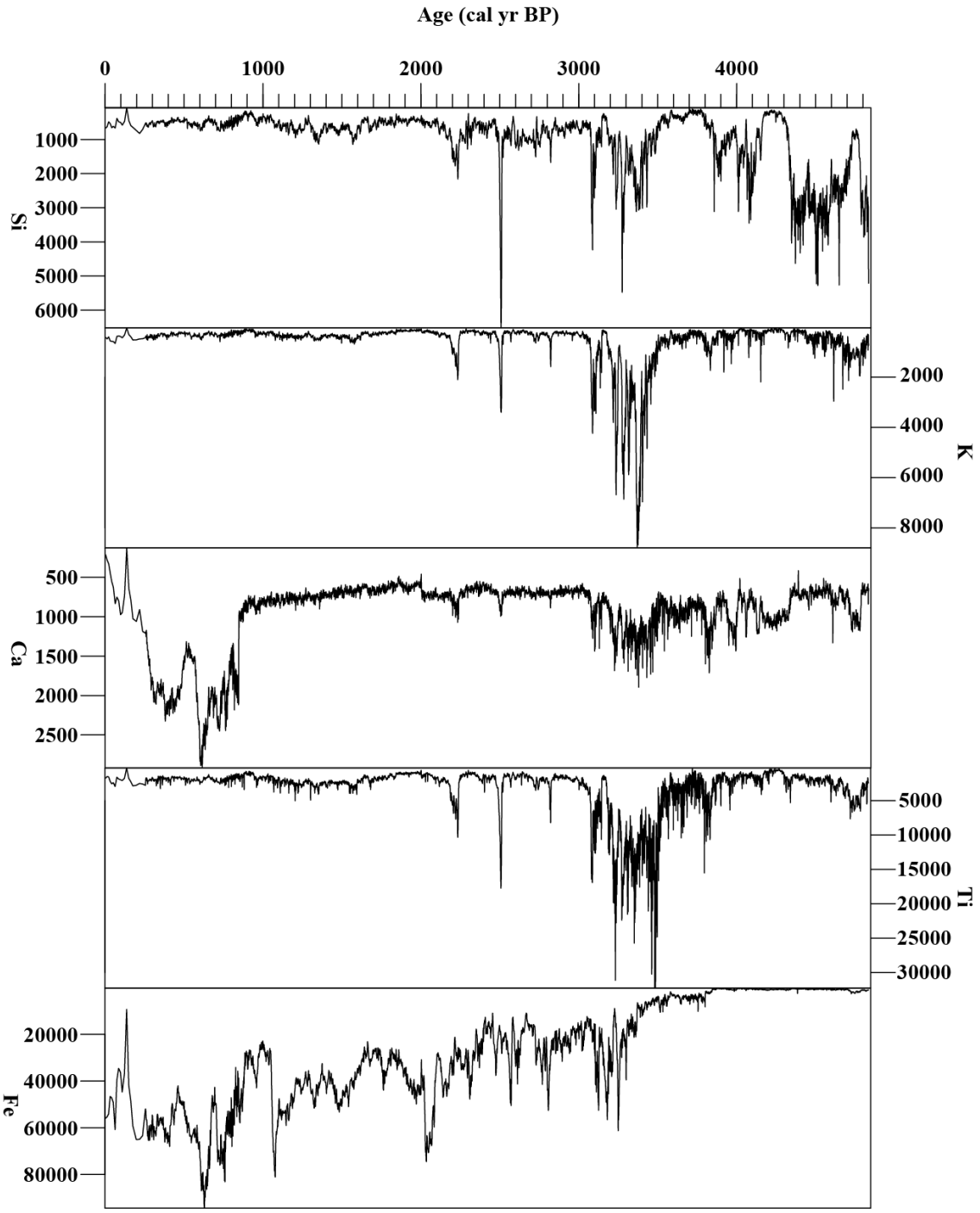

Figure 9: Selected elemental profiles (Si, K, Ca, Ti and Fe) obtained from ITRAX analysis of DWL core.

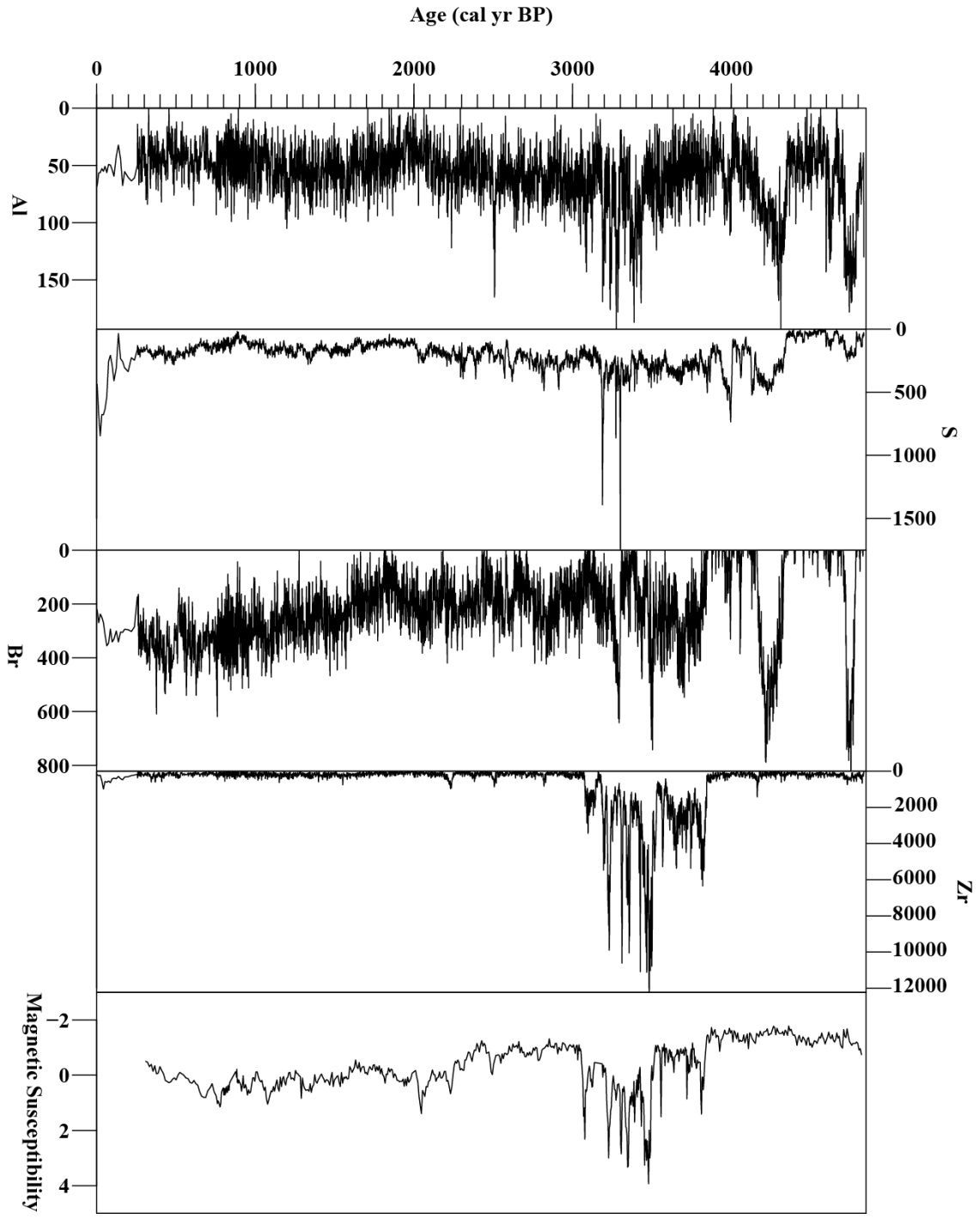

Figure 10: Selected elemental profiles (Al, S, Br and Zr) and magnetic susceptibility obtained from ITRAX analysis of DWL core.

4.9 Magnetic susceptibility

The first 19 cm of sediment had no magnetic susceptibility readings due to the discrete nature of the samples collected from the extruded core. At the base of the core, there is a period from 4800-3800 cal BP, where magnetic susceptibility remains under -1 (Figure 10). From 3800-3500 cal BP, magnetic readings begin to increase. They maintain an average reading of 0, before spiking to a maximum value of 4 with an average of 1-2 from 3500-3000 cal BP. For the remaining 3000-250 cal BP period, the magnetic susceptibility remains relatively constant, with values between -1 and 1 (Figure 10).

5. DISCUSSION

5.1 Chronology

The six ^{210}Pb dates, along with the five radiocarbon dates from the DWL core, show a sediment accumulation rate that remains mostly constant throughout the 5000 year period (Figure 6C). This gives us increased confidence in using the sediment record of DWL for climate and environmental reconstruction over this time period.

The radiocarbon samples vary in the type of material used for dating the core. Identifiable remains from terrestrial plants are the best source for age-depth modelling as the fixed carbon can be constrained to atmospheric CO_2 (Lowe and Walker, 2014). Moreover, where material is identifiable then some assessment can be made of the likelihood that it was deposited soon after death (e.g. as is the case with leaves, but is not the case with charcoal). This was not always possible for DWL, as organic matter was not consistently high enough, and individual organic samples could not be taken. Therefore, the age-depth model is constructed from two radiocarbon dates sourced from bulk sediments and the remainder from terrestrial organics.

5.2 Evidence from charcoal

There are two distinct zones in the charcoal record that suggests a change in fire regimes: The first, a mid-Holocene interval of high, local fire frequency from 4800-4000 cal BP, and a late Holocene interval with decreasing fire evidence from 4000-200 cal BP. There is also a small increase in charcoal from 3800-3000 cal BP, potentially indicating a period of increased regional fire events (Figure 7).

Indigenous Australians have inhabited Fraser Island since the early Holocene, therefore any impact aboriginal settlement may have had on the charcoal record would be prevalent throughout the entire record. European settlement on Fraser Island only began in the late 1800's. Therefore, any impact on fire frequency and vegetation changes at DWL would be small in this record. The majority of logging and mining also occurred at the southern part of the island (Donders et al., 2006), and so is unlikely to affect the DWL catchment. This is backed up with a lack of significant charcoal found in the most recent lake sediments (Figure 7).

5.3 Evidence from carbon isotopes and organic matter

Changes in $\delta^{13}C$ values have been used to reconstruct changes in vegetation and primary productivity (M J. Leng and Henderson, 2013). In oligotrophic lakes $\delta^{13}C$ is correlated with algal productivity due to the photosynthetic demand for dissolved carbon dioxide (J. Williams et al., 2015). $\delta^{13}C$ can also be used to discriminate between different types of land plants through differences in the C_3 and C_4 ^{13}C discrimination. C_3 plants discriminate against ^{13}C to produce shifts of ~ 20‰ in their organic matter (P A. Meyers, 1994). Plants that utilise the C_4 pathway produce shifts of ~ 7‰ in their organic matter (P A. Meyers, 1994).

This enables us to differentiate between C_3 and C_4 plants. C_3 on average, produce $\delta^{13}C$ values of approximately -28‰, and C_4 plants produce $\delta^{13}C$ values of approximately -14‰ (O'Leary, 1988).

The C/N ratio in sediments is representative of the source of organic matter, with aquatic organic matter showing C/N ratio of 10, while terrestrial organic matter has higher than 10 due to the structural C compounds in the higher plants (P A. Meyers, 1994).

The C/N ratio of the DWL sediments fluctuate between 4800-3800 cal BP, indicating a changing source of organic matter into the lake. From 3800-3500 cal BP, the C/N ratio drops to below 15, indicating a shift from terrestrial sources to more within-lake algal sources of lake organic carbon during the mid-Holocene (P A Meyers and Teranes, 2002). This could be due to increased lake nutrient inputs which promote algal growth, or a decrease in soil and vegetation derived organic matter input from the lake catchment (Roberts et al., 2016). From 3500-800 cal BP the C/N ratio stabilises around 20, as the input of terrestrial and aquatic organic matter evens out and remains consistent through the record.

The carbon isotope values in the DWL record are very negative, with $\delta^{13}C$ ranging between -33.6 to -26.9 indicating the organic carbon in DWL is composed of a majority of C_3 vegetation types (O'Leary, 1988).

The resolution of the carbon isotope and C/N data is lower than the other analysis done on DWL, but shows trends in organic content that are accurately correlated with trends in LOI and ITRAX-based estimates of organic matter (i.e. Coh/Inc).

5.4 Evidence from elemental geochemistry

The amount of Ti and other detrital elements, such as K, Fe, and Zr, provide evidence for catchment erosion, or increased movement of allochthonous sediment into the lake (Roberts et al., 2016). The Ti, K and Zr counts all show large, sharp peaks from 3700-3100 cal BP, indicative of a large amount of erosion and input of detrital sediment occurring at this time. This sediment input can be controlled by a range of environmental processes, such as wind erosion and stream runoff (Martin-Puertas et al., 2012). The amount of stream runoff is dominantly controlled by variations in precipitation, with higher rainfall washing increasing amounts of sediment from the catchment into the lake system. The amount of wind erosion is often controlled by changes in vegetation, with increasing erosion occurring in response to a lack of vegetation.

The Fe influx in the DWL sediment from 3500 cal BP to present, appears independent of the other detrital elements, potentially indicative of a reduction and oxidation relationship in the more recent lake sediments.

The Si peaks in the sediments is representative of sand content in the core, with high values visible from the base of the core (4800 cal BP) to 3800 cal BP. The increased Si content from 4800-3800 cal BP is not largely represented in any of the other elemental profiles, indicating that this influx of sand was not caused by an increase in erosion. From 3500 cal BP to present, Si follows the same trends as the detrital based elements, indicating erosion based control from this point onwards.

The elemental profile for Ca remains constant up until 900 cal BP, where there is a large peak that gradually decreases until present time. This peak in Ca could potentially be

linked to an increase in calcium carbonate precipitation or an influx of detrital carbonates into the lake.

5.5 Magnetic susceptibility

Magnetic susceptibility readings can be used to determine a range of depositional processes. Magnetic susceptibility can be used to detect allochthonous input that is often associated with fire events as a result of erosion (Oldfield et al., 1999; Thompson, 2012). Minor peaks in magnetic susceptibility, which are not associated with charcoal peaks have been inferred to be caused by other disturbances of the catchment (Millspaugh and Whitlock, 1995).

The magnetic susceptibility of DWL shows three periods of change. The first from 4800-3900 cal BP is characterised by values of -1. The values of -1 corresponds with very low Fe values and a mixture of high silica content and high organic matter in the core, as they are diamagnetic, and exhibit negative magnetic susceptibility readings (Li et al., 2014). This period of low magnetic is also characterised by a peak period of charcoal.

Magnetic susceptibility then peaks from 3900-3000 cal BP, along with peaks within detrital elements (Ti, K and Zr). Magnetic susceptibility then decreases and maintains values between -1 and 1, as detrital influx remains steady and there are no additional large inputs of Si and organic matter.

5.6 Environmental change and lake response

The analysis of the multiple proxy evidence allows the reconstruction of environmental changes in Deepwater Lake and its surrounding catchment over the 4800 cal BP sediment history (Figure 11 and 12).

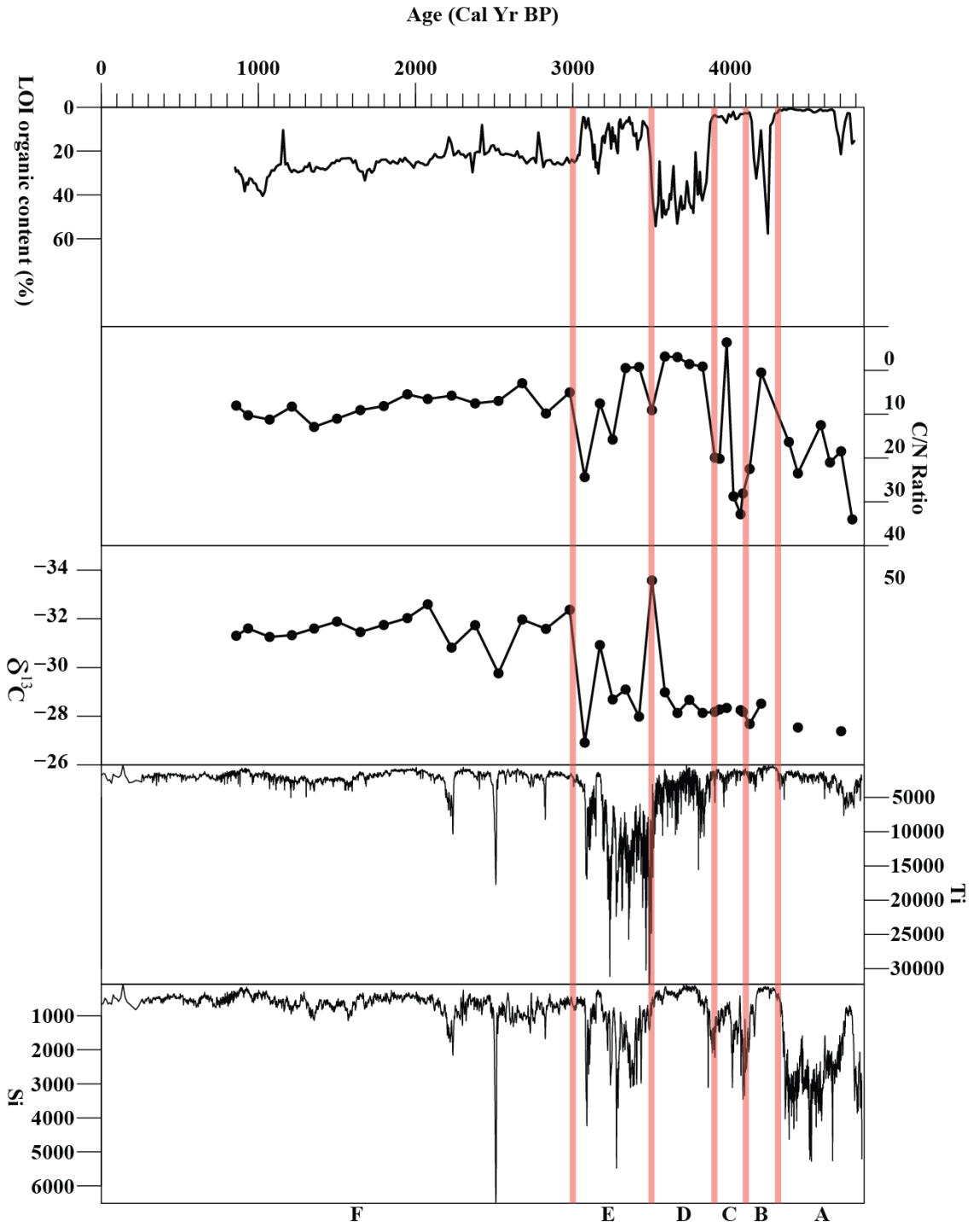

Figure 11. Summary diagram showing selected data sets (Organic content, C/N ratio, $\delta^{13}C$, Ti/cps and Si/cps). Overlain in red are 5 periods where change is visible in many of the data sets. A: 4800-4300 cal BP. B: 4300-4100 cal BP C: 4100-3900 cal BP D: 3900-3500 cal BP E: 3500-3000 cal BP F: 3000 cal BP to present

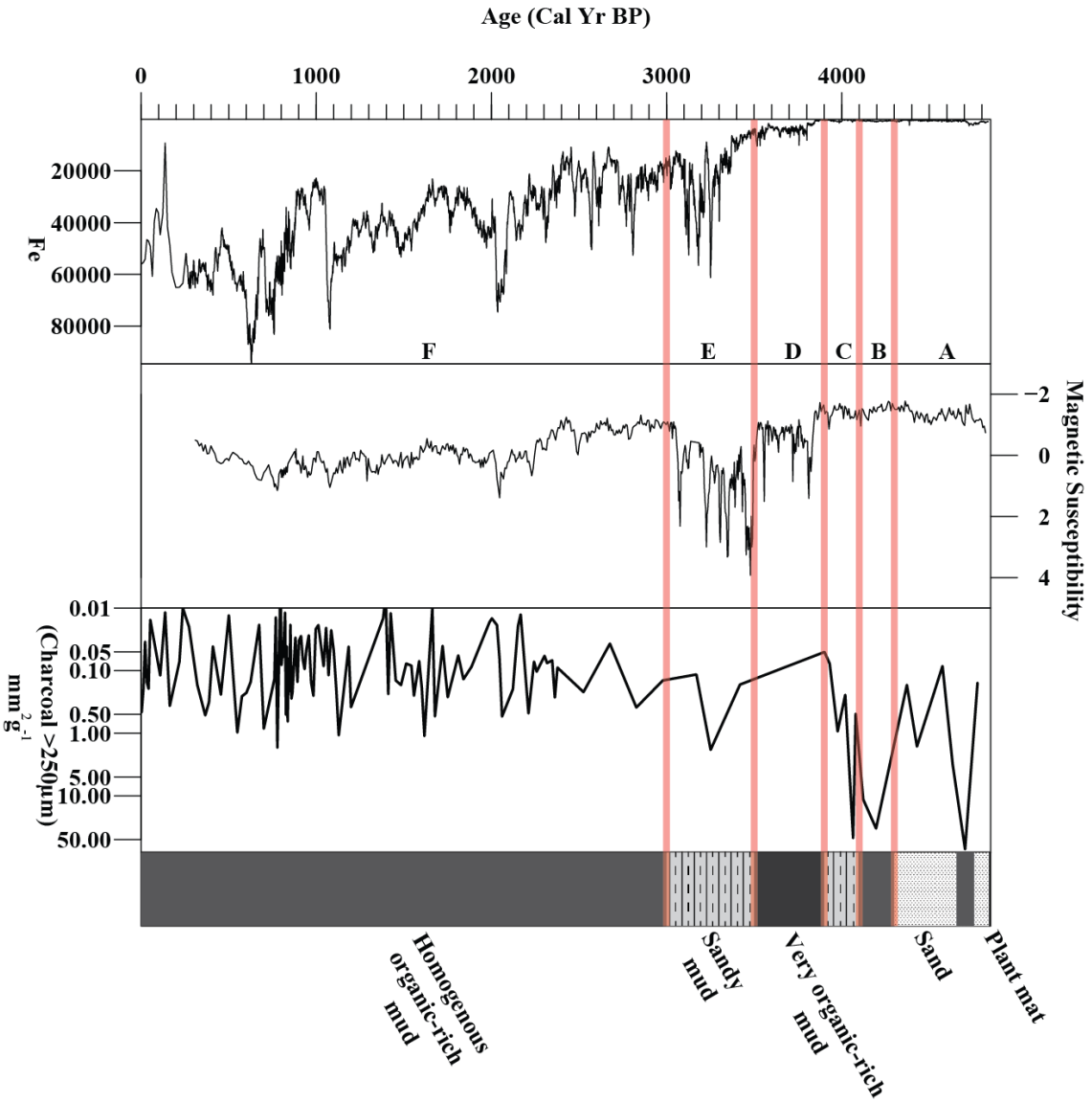

Figure 12: Summary diagram showing selected data sets (Fe/cps, magnetic susceptibility, >250 µm charcoal mm^2g^{-1} and lithological description). Overlain in red are 5 periods where change is visible in many of the data sets. A: 4800-4300 cal BP. B: 4300-4100 cal BP C: 4100-3900 cal BP D: 3900-3500 cal BP E: 3500-3000 cal BP F: 3000 cal BP to present

5.6.1 PERIOD A (4800-4300 CAL BP)

Beginning from 4800 cal BP, at the base of the core there is a fibrous plant mat with long "hair-like" fibres (Figure 12). From 4800-4300 cal BP, the sediment has almost no organic matter and is instead dominated by sand (Si). There is a very large period of peak charcoal within this period, suggesting that there was an increase in local fire events during this period, showing potential links to drought conditions through the

mid-Holocene. The C/N ratio of >20 indicates that the little organic matter that is found at this time is based on a terrestrial source. There are only two recorded $\delta^{13}C$ values during the period, due to very low organic content, but the two values are generally high, around -27‰ indicating organic input is dominated by C_3 vegetation. Magnetic susceptibility values during this period are consistently less than -1, very likely due to an increase in amount of sand found in the core, as shown by the Si content and optical images of the sediment.

These findings indicate a period of large environmental change, perhaps with increased wind strength, providing transport for sand and macro-charcoal into the lake. This interpretation is supported by the aeolian sedimentation records from Native Companion Lagoon on North Stradbroke Island, which indicates widespread wind erosion during this period, of a magnitude only exceeded during the last glacial maximum (McGowan et al., 2008). High levels of charcoal deposition are also evident at nearby Lake Allom on Fraser Island during this time period (Donders et al., 2006). It is also possible that the large amount of sand in this portion of the sediment record is indicative of the early creation of the lake. With the mid-Holocene being categorised as a "dry" period (Longmore, 1997b), it is possible that there may not have been a lake at all during this time, with the lake developing in period B and C.

5.6.2 PERIOD B (4300-4100 CAL BP)

After 4300 cal BP, there is a small peak in organic content in the sediment. The C/N ratio decreases to 10, indicating a short transition from a majority of allochthonous input of terrestrial plant material into a higher proportion of aquatic based sources of carbon. There is still a peak period in charcoal indicating a possible increase in local fire events, sending increased charcoal from the catchment into the lake.

Magnetic susceptibility remains constant, while sand content (Si) drops rapidly. A decrease in sand content is consistent with some studies from the nearby North Stradbroke Island (NSI), which suggest decreasing sand deposition from 5000-4000 cal B2K (Barr et al., 2013). This is not supported by others, who found continued sand deposition and increasing charcoal deposition during the same time (McGowan et al., 2008).

5.6.3 PERIOD C (4100-3900 CAL BP)

From 4100-3900 cal BP, organic content declines to almost zero. The C/N ratio at this time varies, potentially transitioning from terrestrial to aquatic sources and back again during this period. $\delta^{13}C$ values remain constant at -28‰ consistent with a C_3 dominated vegetation during this period. The charcoal record begins to decrease during this period, almost completely disappearing by 3900 cal BP. The sand content (Si) returns, suggesting the brief period B was a singular event and not an indication of a large scale environmental change during this time. The high sand content along with a decreasing charcoal content towards the end of period C is likely due to similar conditions experienced at period A, with increased aeolian transport and erosion.

5.6.4 PERIOD D (3900-3500 CAL BP)

From 3900-3500 cal BP, there is a significant change in environmental conditions, seen from an increase in organic content and a large input of detrital elements. Unusually, the $\delta^{13}C$ values remain at -28‰, with the C/N ratio decreasing from >30 to <10. The decrease of C/N ratio to values below 10 is often indicative of an aquatic based organic input such as algae or macrophytes. Algae and macrophytes generally have low $\delta^{13}C$ values due to the preferential uptake of ^{13}C depleted carbon from lake water (M J Leng

et al., 2006), and so this relationship is difficult to explain. However this relationship could be due to an increase in C_4 organic matter input into the lake, increasing the $\delta^{13}C$ values, as C_4 plants demonstrate much higher $\delta^{13}C$ values (-13 $\delta^{13}C$), and countering the effect of an increased algal based organic input. It is difficult to see small-scale vegetation changes from other records on Fraser Island as they focus on large time scales from the late Pleistocene to the Holocene.

Beginning at 3900 cal BP, the appearance of many detrital based elements begin to increase in the core. Ti, K and Zr begin to increase during this time, likely driven by an increase in erosion caused by high rainfall levels. Organic content increase to 40%, consistent with periods of high precipitation and promoted growth. Increased precipitation would help wash detrital sediments and organics into the lake from the catchment (Martin-Puertas et al., 2012). Magnetic susceptibility also increases at this time, with the disappearance of the majority of sand and an increase in detrital elements driving this change.

Interestingly, charcoal shows large decreases in the record during this time, meaning any erosion was likely not driven by an increased fire regime. The disappearance of charcoal can also be explained by the increase in rainfall and moisture content. The disappearance of charcoal particles in the >125 μm size range is supported by very few particles present in sediments recorded from Lake Allom (Donders et al., 2006).

5.6.5 PERIOD E (3500-3000 CAL BP)

From 3500-3000 cal BP, organic content and TOC decreases to 10%, along with a gradual increase of the C/N ratio, from aquatic dominated sources (<10), to more

terrestrial based (>30) sediments. The $\delta^{13}C$ fluctuates slightly, from between -34‰ to -27‰, indicating a minor shift in terrestrial to aquatic organic sources.

Detrital element input also increases further as the period moves towards 3000 cal BP, indicating an even higher amount of erosion following from period D (Figure 11 and 12). Similarly this can be seen in the magnetic susceptibility readings, which increase along with the detrital elements.

The increase in C/N ratio and shift to more terrestrial based organic sources aligns with the beginning of the rapid expansion of rainforest taxa from 3500 cal BP onwards (Donders et al., 2006).

5.6.6 PERIOD F (3000-0 CAL BP)

The final period from 3000 cal BP to present shows very little variation in all proxies. Indicating a period of remarkable stability for the region. There are no significant fluctuations in detrital input or charcoal indicating little to no erosion bringing in sediments. Organic content remains constant between 20-30%, indicating a steady amount of organic matter input into the lake, which appears to be largely terrestrial based on a C/N ratio of 20. $\delta^{13}C$ remains steady at -31‰, indicating the rainforests are dominated by species showing C_3 photosynthesis. Sand in the lake during this time period remains relatively constant, indicating a constant rate of aeolian sediment influx, consistent with the findings of McGowan et al. (2008) of nearly constant deposition of wind transported sediments. Fire frequency remains low throughout this period, which is unexpected, as the frequency of El Niño events was at its highest during this period (Moy et al., 2002). The rapid development of a rainforest dominated system during this time can assist in explaining the decreasing rate of erosion and fire as many species of

trees begin to appear in the pollen record from 2500 cal BP onwards (Donders et al., 2006). Evidence for human impact in the form of changing fire activity is absent from the DWL record. This is in contrast with lake records from North Stradbroke Island where increased burning is detected from mid to late-Holocene and linked with increasing human activity (Moss et al., 2013).

5.7 Future work

Charcoal, geochemistry, and stable isotopes all provide a consistent multi-proxy reconstruction of the past climate on Fraser Island. However the addition of diatom and pollen values from the lake could help better constrain past climate conditions.

Improving the chronology of DWL is one of the next steps in constraining changes within the sediment core. Additional ^{210}Pb age data points, with independent checking using Pu or ^{137}Cs, will help improve the chronology of DWL, allowing a more accurate age-depth model to be constructed.

Further research into the other lakes on Fraser Island will also assist to fill in gaps in the current climate model for Fraser Island, with particular focus over the mid-late Holocene.

6. CONCLUSIONS

Through the analysis of a sediment core from Deepwater Lake, with the use of multiple proxies, past climate and environmental conditions over the mid- to late-Holocene have been reconstructed.

The geochemical analysis of lake sediments revealed records of erosion and detrital sediment influx into the lake sediments. Organic matter analysis revealed changes in source organic matter, including a transition period from majority terrestrial source, to a

300 year period of aquatic dominated organic input. A fire abundance record demonstrated an almost complete drop-off of charcoal input into the lake past 4000 cal BP, indicative of a transition from drought conditions into a higher moisture environment with lower fire frequency.

The reconstruction shows a marked shift from a dry mid-Holocene period from 4800-3900 cal BP with high fire frequency and large amounts of aeolian sediment transport, into a wetter late-Holocene period from 3900-3100 cal BP with large amounts of detrital sediment input likely driven by increases in precipitation. From 3000 cal BP to present, environmental conditions remain consistently stable coinciding with rapid expansion of rainforest taxa (Donders et al., 2006). The reconstruction shows the transition out of the dry mid-Holocene earlier than presented in Longmore (1997), possibly due to differences in lake morphology and local environmental conditions surrounding the different lake systems.

ACKNOWLEDGMENTS

I would firstly like to thank my supervisors, Dr Francesca McInerney, Dr John Tibby and Dr Jonathan Tyler for the opportunity to undertake my honours program, along with their full support and guidance over the past year.
For support for field work costs, I would like to thank the University of Adelaide's Environment Institute.
The team who collected the DWL core: Jonathan Marshall, Glenn McGregor and Cameron Schultz from Department of Science, Information Technology and Innovation, along with Cameron Barr, Francesca McInerney, Haidee Cadd and John Tibby from The University of Adelaide.
I would like to thank ANSTO portal grant 10932, which supported the ^{210}Pb and ^{14}C dating along with the ITRAX core scanning. Thanks to Geraldine Jacobsen, Sabika Maizma, Atun Zawadzki, Patricia Gadd and everyone at ANSTO who assisted.
I would also like to thank Prof. Melanie Leng at the British Geological Survey for her work on the carbon isotope and C/N ratio samples.
Thanks to both Cesca's and Jon's lab groups for their assorted assistance throughout the year, both in the lab and with writing.
I would finally like to thank my family and fellow honours students for their support, with special thanks to Claire Murphy for helping with lab work throughout the year.

REFERENCES

APPLEBY, P. G. (2001). Chronostratigraphic Techniques in Recent Sediments. In W. M. Last & J. P. Smol (Eds.), *Tracking Environmental Change Using Lake Sediments: Basin Analysis, Coring, and Chronological Techniques* (pp. 171-203). Dordrecht: Springer Netherlands.

ATAHAN, P., HEIJNIS, H., DODSON, J., GRICE, K., LE MÉTAYER, P., TAFFS, K., . . . ZAWADZKI, A. (2015). Pollen, biomarker and stable isotope evidence of late Quaternary environmental change at Lake McKenzie, southeast Queensland. *Journal of Paleolimnology, 53*(1), 139-156. doi:10.1007/s10933-014-9813-3

BARR, C., TIBBY, J., MARSHALL, J. C., MCGREGOR, G. B., MOSS, P. T., HALVERSON, G. P., & FLUIN, J. (2013). Combining monitoring, models and palaeolimnology to assess ecosystem response to environmental change at monthly to millennial timescales: the stability of Blue Lake, North Stradbroke Island, Australia. *Freshwater Biology, 58*(8), 1614-1630. doi:10.1111/fwb.12154

BLAAUW, M., & CHRISTEN, J. A. (2011). Flexible paleoclimate age-depth models using an autoregressive gamma process. *Bayesian Anal., 6*(3), 457-474. doi:10.1214/11-BA618

BLACK, M. P., MOONEY, S. D., & MARTIN, H. A. (2006). A >43,000-year vegetation and fire history from Lake Baraba, New South Wales, Australia. *Quaternary Science Reviews, 25*(21), 3003-3016. doi:https://doi.org/10.1016/j.quascirev.2006.04.006

BOM, A. B. O. M. (2017). Climate Statistics for Australian Locations. Retrieved from http://www.bom.gov.au/climate/averages/tables/cw_039085.shtml

BRADSTOCK, R. A. (2010). A biogeographic model of fire regimes in Australia: current and future implications. *Global Ecology and Biogeography, 19*(2), 145-158. doi:10.1111/j.1466-8238.2009.00512.x

BURNETT, A. P., SOREGHAN, M. J., SCHOLZ, C. A., & BROWN, E. (2011). Tropical East African climate change and its relation to global climate: A record from Lake Tanganyika, Tropical East Africa, over the past 90+kyr. *Palaeogeography, Palaeoclimatology, Palaeoecology, 303*(1), 155-167. doi:https://doi.org/10.1016/j.palaeo.2010.02.011

DONDERS, T. H., WAGNER, F., & VISSCHER, H. (2006). Late Pleistocene and Holocene subtropical vegetation dynamics recorded in perched lake deposits on Fraser Island, Queensland, Australia. *Palaeogeography, Palaeoclimatology, Palaeoecology, 241*(3–4), 417-439. doi:https://doi.org/10.1016/j.palaeo.2006.04.008

EMILE-GEAY, J., COBB, K. M., MANN, M. E., & WITTENBERG, A. T. (2013). Estimating Central Equatorial Pacific SST Variability over the Past Millennium. Part II: Reconstructions and Implications. *Journal of Climate, 26*(7), 2329-2352. doi:10.1175/JCLI-D-11-00511.1

FINK, D., HOTCHKIS, M., HUA, Q., JACOBSEN, G., SMITH, A. M., ZOPPI, U., . . . WILLIAMS, M. (2004). The ANTARES AMS facility at ANSTO. *Nuclear Instruments and Methods in Physics Research Section B: Beam Interactions with Materials and Atoms, 223*, 109-115. doi:http://dx.doi.org/10.1016/j.nimb.2004.04.025

GADD, P. (2016). *Can the Molybdenum Incoherent/Molybdenum Coherent scattering ratio (Mo Ratio) be used as a substitute for LOI determinations of organic content?* Paper presented at the AQUA 2016 biennial meeting, University of Auckland.

GONTZ, A. M., MOSS, P. T., SLOSS, C. R., PETHERICK, L. M., MCCALLUM, A., & SHAPLAND, F. (2015). Understanding past climate variation and environmental change for the future of an iconic landscape – K'gari Fraser Island, Queensland, Australia. *Australasian Journal of Environmental Management, 22*(2), 105-123. doi:10.1080/14486563.2014.1002120

HEIRI, O., LOTTER, A. F., & LEMCKE, G. (2001). Loss on ignition as a method for estimating organic and carbonate content in sediments: reproducibility and comparability of results. *Journal of Paleolimnology, 25*(1), 101-110. doi:10.1023/a:1008119611481

HEMBROW, S. C., TAFFS, K. H., ATAHAN, P., PARR, J., ZAWADZKI, A., & HEIJNIS, H. (2014). Diatom community response to climate variability over the past 37,000years in the sub-tropics of the Southern Hemisphere. *Science of The Total Environment, 468*(Supplement C), 774-784. doi:https://doi.org/10.1016/j.scitotenv.2013.09.003

HOGG, A. G., HUA, Q., BLACKWELL, P. G., NIU, M., BUCK, C. E., GUILDERSON, T. P., . . . ZIMMERMAN, S. R. H. (2016). SHCal13 Southern Hemisphere Calibration, 0–50,000 Years cal BP. *Radiocarbon, 55*(4), 1889-1903. doi:10.2458/azu_js_rc.55.16783

LEES, B. (2006). Timing and Formation of Coastal Dunes in Northern and Eastern Australia. *Journal of Coastal Research*, 78-89. doi:10.2112/05a-0007.1

LENG, M. J., & HENDERSON, A. C. G. (2013). Recent advances in isotopes as palaeolimnological proxies. *Journal of Paleolimnology, 49*(3), 481-496. doi:10.1007/s10933-012-9667-5

LENG, M. J., LAMB, A. L., HEATON, T. H., MARSHALL, J. D., WOLFE, B. B., JONES, M. D., . . . ARROWSMITH, C. (2006). Isotopes in lake sediments *Isotopes in palaeoenvironmental research* (pp. 147-184): Springer.

LI, Y., ZUO, R., BAI, Y., & YANG, M. (2014). The relationships between magnetic susceptibility and elemental variations for mineralized rocks. *Journal of Geochemical Exploration, 146*(Supplement C), 17-26. doi:https://doi.org/10.1016/j.gexplo.2014.07.010

LONG, C. J., WHITLOCK, C., BARTLEIN, P. J., & MILLSPAUGH, S. H. (1998). A 9000-year fire history from the Oregon Coast Range, based on a high-resolution charcoal study. *Canadian Journal of Forest Research, 28*(5), 774-787. doi:10.1139/x98-051

LONGMORE, M. E. (1997a). Quaternary Palynological Records from Perched Lake Sediments, Fraser Island, Queensland, Australia: Rainforest, Forest History and Climatic Control. *Australian Journal of Botany, 45*(3), 507-526. doi:https://doi.org/10.1071/BT96109

LONGMORE, M. E. (1997b). The mid-Holocene" Dry" Anomaly on the Mid-Eastern Coast of Australia: Calibration of Palaeowater Depth as a Surrogate for Effective Precipitation using Sedimentary Loss on Ignition in the Perched Lake Sediments of Fraser island, Queensland. *Palaeoclimates, 4*, 1-26.

LONGMORE, M. E., & HEIJNIS, H. (1999). Aridity in Australia: Pleistocene records of Palaeohydrological and Palaeoecological change from the perched lake sediments of Fraser Island, Queensland, Australia. *Quaternary International, 57*, 35-47. doi:http://dx.doi.org/10.1016/S1040-6182(98)00048-2

LOURENSZ, R. S. (1981). *Tropical cyclones in the Australian region, July 1909 to June 1980*. Canberra: Australian Government Publishing Service.

LOWE, J. J., & WALKER, M. J. (2014). *Reconstructing quaternary environments*: Routledge.

MARTIN-PUERTAS, C., BRAUER, A., DULSKI, P., & BRADEMANN, B. (2012). Testing climate–proxy stationarity throughout the Holocene: an example from the varved sediments of Lake Meerfelder Maar (Germany). *Quaternary Science Reviews, 58*, 56-65. doi:https://doi.org/10.1016/j.quascirev.2012.10.023

MCGOWAN, H. A., PETHERICK, L. M., & KAMBER, B. S. (2008). Aeolian sedimentation and climate variability during the late Quaternary in southeast Queensland, Australia. *Palaeogeography, Palaeoclimatology, Palaeoecology, 265*(3), 171-181. doi:https://doi.org/10.1016/j.palaeo.2008.05.011

MEYERS, P. A. (1994). Preservation of elemental and isotopic source identification of sedimentary organic matter. *Chemical Geology, 114*(3), 289-302. doi:https://doi.org/10.1016/0009-2541(94)90059-0

MEYERS, P. A., & TERANES, J. L. (2001). Sediment organic matter. In W. M. Last & J. P. Smol (Eds.), *Tracking Environmental Change Using Lake Sediments. Volume 2: Physical and Geochemical Methods* (Vol. 2, pp. 239-269): Springer Netherlands.

MEYERS, P. A., & TERANES, J. L. (2002). Sediment organic matter. *Tracking environmental change using lake sediments*, 239-269.

MILLSPAUGH, S. H., & WHITLOCK, C. (1995). A 750-year fire history based on lake sediment records in central Yellowstone National Park, USA. *The Holocene, 5*(3), 283-292. doi:10.1177/095968369500500303

MOONEY, S., & BLACK, M. (2003). A simple and fast method for calculating the area of macroscopic charcoal isolated from sediments. *Quaternary Australasia, 21*(1), 18-21.

MOONEY, S., & RADFORD, K. (2001). A simple and fast method for the quantification of macroscopic charcoal from sediments. *Quaternary Australasia, 19*, 43-46.

MOSS, P. T., TIBBY, J., PETHERICK, L., MCGOWAN, H., & BARR, C. (2013). Late Quaternary vegetation history of North Stradbroke Island, Queensland, eastern Australia. *Quaternary Science Reviews, 74*(Supplement C), 257-272. doi:https://doi.org/10.1016/j.quascirev.2013.02.019

MOY, C. M., SELTZER, G. O., RODBELL, D. T., & ANDERSON, D. M. (2002). Variability of El Niño/Southern Oscillation activity at millennial timescales during the Holocene epoch. *Nature, 420*(6912), 162.

MURPHY, B. F., & RIBBE, J. (2004). Variability of southeastern Queensland rainfall and climate indices. *International Journal of Climatology, 24*(6), 703-721. doi:10.1002/joc.1018

MURPHY, B. F., & TIMBAL, B. (2008). A review of recent climate variability and climate change in southeastern Australia. *International Journal of Climatology, 28*(7), 859-879. doi:10.1002/joc.1627

MURPHY, B. P., BRADSTOCK, R., BOER, M. M., CARTER, J., CARY, G. J., COCHRANE, M. A., . . . BOWMAN, D. M. J. S. (2013). Fire regimes of Australia: a pyrogeographic model system. *Journal of Biogeography, 40*(6), 1048-1058. doi:10.1111/jbi.12065

O'LEARY, M. H. (1988). Carbon isotopes in photosynthesis. *BioScience, 38*(5), 328-336.

OLDFIELD, F., WALDEN, J., & SMITH, J. (1999). *Environmental magnetism: a practical guide*: Quaternary Research Association.

RISBEY, J. S., POOK, M. J., MCINTOSH, P. C., WHEELER, M. C., & HENDON, H. H. (2009). On the Remote Drivers of Rainfall Variability in Australia. *Monthly Weather Review, 137*(10), 3233-3253. doi:10.1175/2009MWR2861.1

ROBERTS, N., ALLCOCK, S. L., ARNAUD, F., DEAN, J. R., EASTWOOD, W. J., JONES, M. D., . . . YIĞITBAŞIOĞLU, H. (2016). A tale of two lakes: a multi-proxy comparison of Lateglacial and Holocene environmental change in Cappadocia, Turkey. *Journal of Quaternary Science, 31*(4), 348-362. doi:10.1002/jqs.2852

RUSSELL-SMITH, J., YATES, C. P., WHITEHEAD, P. J., SMITH, R., CRAIG, R., ALLAN, G. E., . . . GILL, A. M. (2007). Bushfires down under: patterns and implications of contemporary Australian landscape burning. *International Journal of Wildland Fire, 16*(4), 361-377. doi:https://doi.org/10.1071/WF07018

SCHINDELIN, J., RUEDEN, C. T., HINER, M. C., & ELICEIRI, K. W. (2015). The ImageJ ecosystem: An open platform for biomedical image analysis. *Molecular Reproduction and Development, 82*(7-8), 518-529. doi:10.1002/mrd.22489

SNYDER, C. W. (2010). The value of paleoclimate research in our changing climate. *Climatic Change, 100*(3), 407-418. doi:10.1007/s10584-010-9842-5

TEAM, R. C. (2017). R: A language and enviroment for statistical computing. Vienna, Austria: R Foundation for Statistical Computing. Retrieved from https://www.R-project.org/

THOMPSON, R. (2012). *Environmental magnetism*: Springer Science & Business Media.

TIMMS, B. V. (1986). The Coastal Dune Lakes of Eastern Australia. *Limnology in Australia, 61*, 421-432. doi:10.1007/978-94-009-4820-4_26

TUDHOPE, A. W., SHIMMIELD, G. B., CHILCOTT, C. P., JEBB, M., FALLICK, A. E., & DALGLEISH, A. N. (1995). Recent changes in climate in the far western equatorial Pacific and their relationship to the Southern Oscillation; oxygen isotope records from massive corals, Papua New Guinea. *Earth and Planetary Science Letters, 136*(3), 575-590. doi:https://doi.org/10.1016/0012-821X(95)00156-7

UMMENHOFER, C. C., ENGLAND, M. H., MCINTOSH, P. C., MEYERS, G. A., POOK, M. J., RISBEY, J. S., . . . TASCHETTO, A. S. (2009). What causes southeast Australia's worst droughts? *Geophysical Research Letters, 36*(4), n/a-n/a. doi:10.1029/2008GL036801

VEROSUB, K. L., & ROBERTS, A. P. (1995). Environmental magnetism: Past, present, and future. *Journal of Geophysical Research: Solid Earth, 100*(B2), 2175-2192. doi:10.1029/94JB02713

WILKINS, D., GOURAMANIS, C., DECKKER, P. D., FIFIELD, L. K., & OLLEY, J. (2013). Holocene lake-level fluctuations in Lakes Keilambete and Gnotuk, southwestern Victoria, Australia. *The Holocene, 23*(6), 784-795. doi:10.1177/0959683612471983

WILLIAMS, A. A. J., KAROLY, D. J., & TAPPER, N. (2001). The Sensitivity of Australian Fire Danger to Climate Change. *Climatic Change, 49*(1), 171-191. doi:10.1023/a:1010706116176

WILLIAMS, J., MCLAUCHLAN, K., MUELLER, J., MELLICANT, E., E MYRBO, A., & LASCU, L. (2015). *Ecosystem development following deglaciation: A new sedimentary record from Devils Lake, Wisconsin, USA* (Vol. 125).

WOLTERING, M., ATAHAN, P., GRICE, K., & HEIJNIS, H. (2014). Glacial and Holocene terrestrial temperature variability in subtropical east Australia as inferred from branched GDGT distributions in a sediment core from Lake McKenzie. *Quaternary Research, 82*(1), 132-145. doi: https://doi-org.proxy.library.adelaide.edu.au/10.1016/j.yqres.2014.02.005

WRIGHT JR, H. (1967). A square-rod piston sampler for lake sediments. *Journal of Sedimentary Research, 37*(3).

ZHENGYU, L. (2012). Dynamics of Interdecadal Climate Variability: A Historical Perspective. *Journal of Climate, 25*(6), 1963-1995. doi:10.1175/2011jcli3980.1

APPENDIX A: CORE PHOTOGRAPHS

Drive 1 55-155 cm

Top Base

Drive 2 155-255 cm

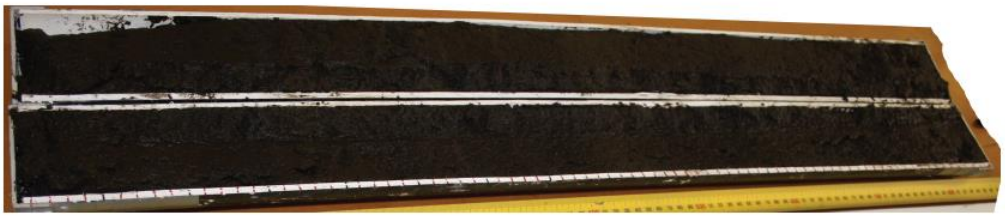

Top Base

Drive 3 255-355 cm

Top Base

Drive 4 355-461 cm

Top Base


Drive 1
55-155 cm
Drive 2
155-255 cm
Drive 3
255-355 cm
Drive 4
355-461 cm
Top
Base

APPENDIX B: ALL ITRAX CORE SCANNER DATA

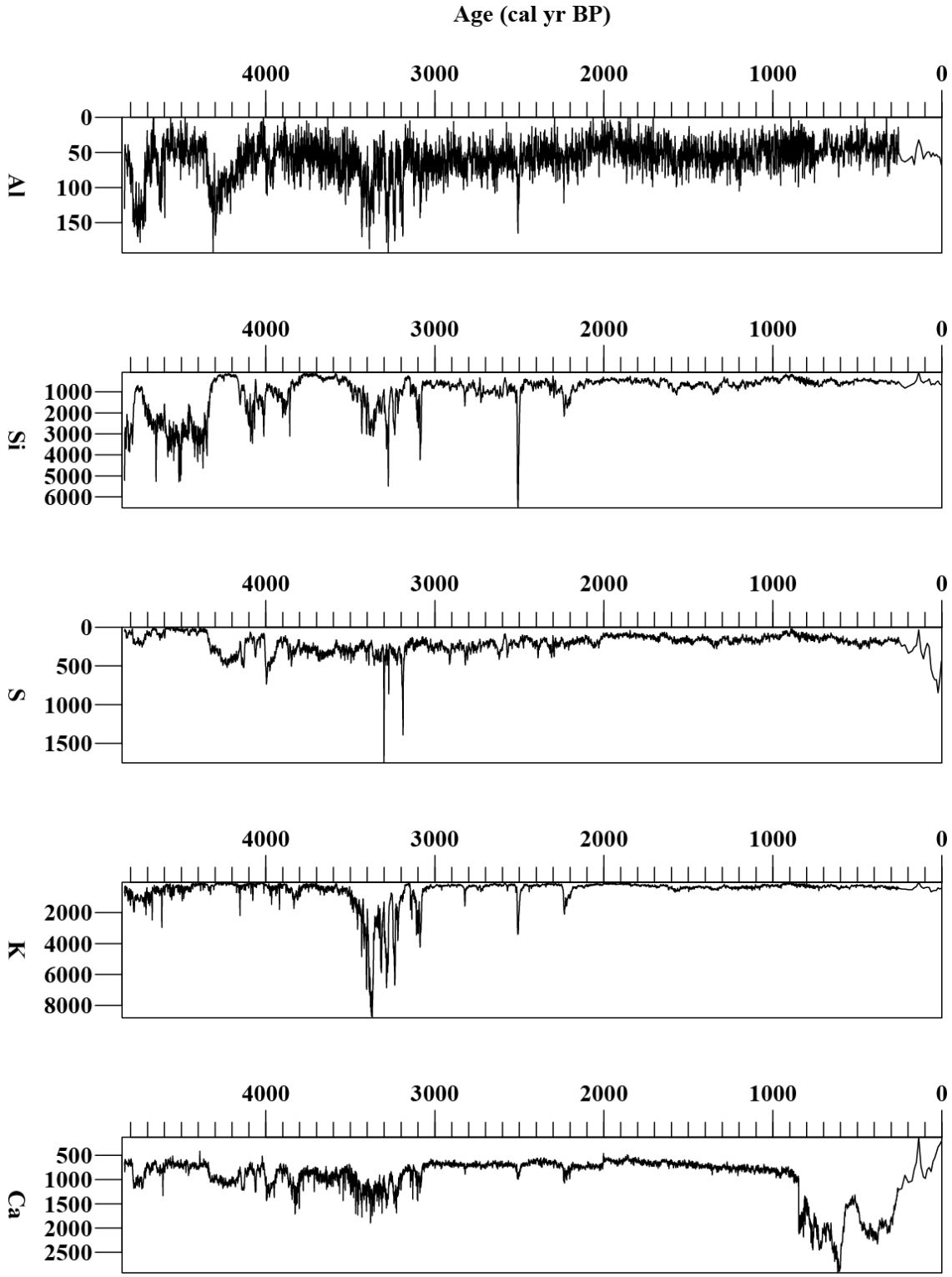

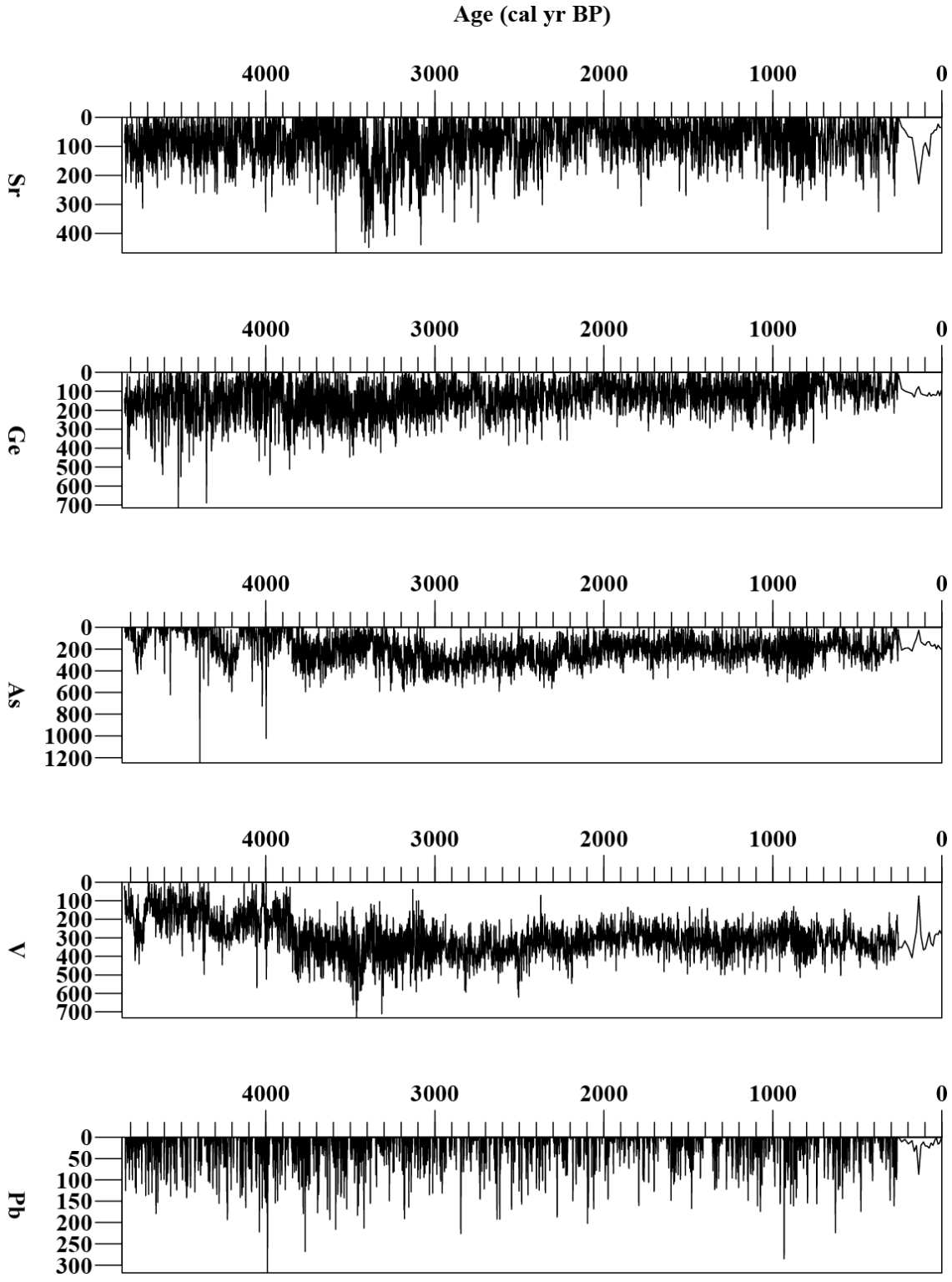
Age (cal yr BP)
4000
3000
2000
1000
0
Sr
0
100
200
300
400
Ge
0
100
200
300
400
500
600
700
As
0
200
400
600
800
1000
1200
V
0
100
200
300
400
500
600
700
Pb
0
50
100
150
200
250
300

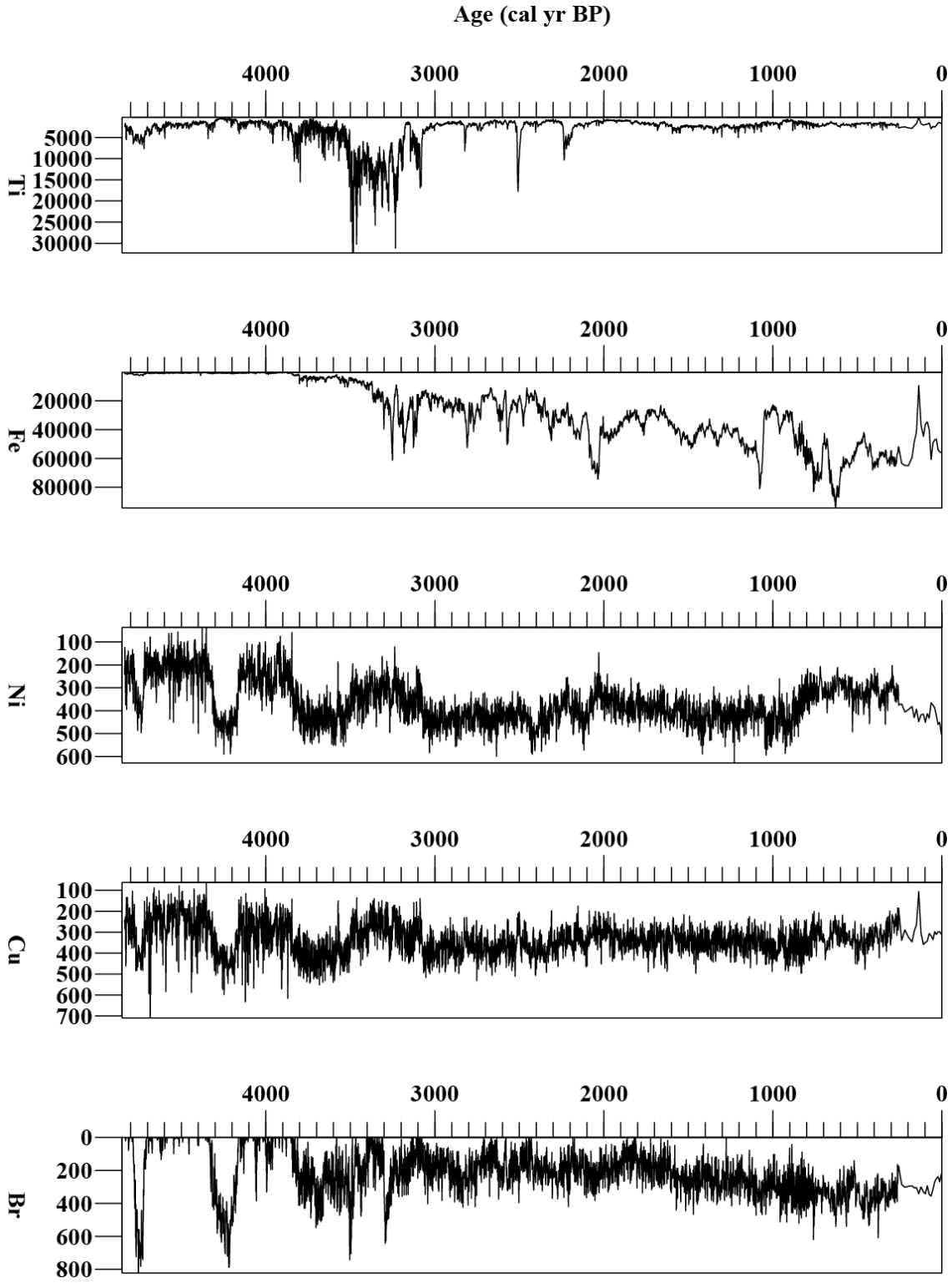
Age (cal yr BP)
4000
3000
2000
1000
0
Ti
5000
10000
15000
20000
25000
30000
Fe
20000
40000
60000
80000
Ni
100
200
300
400
500
600
Cu
100
200
300
400
500
600
700
Br
0
200
400
600
800

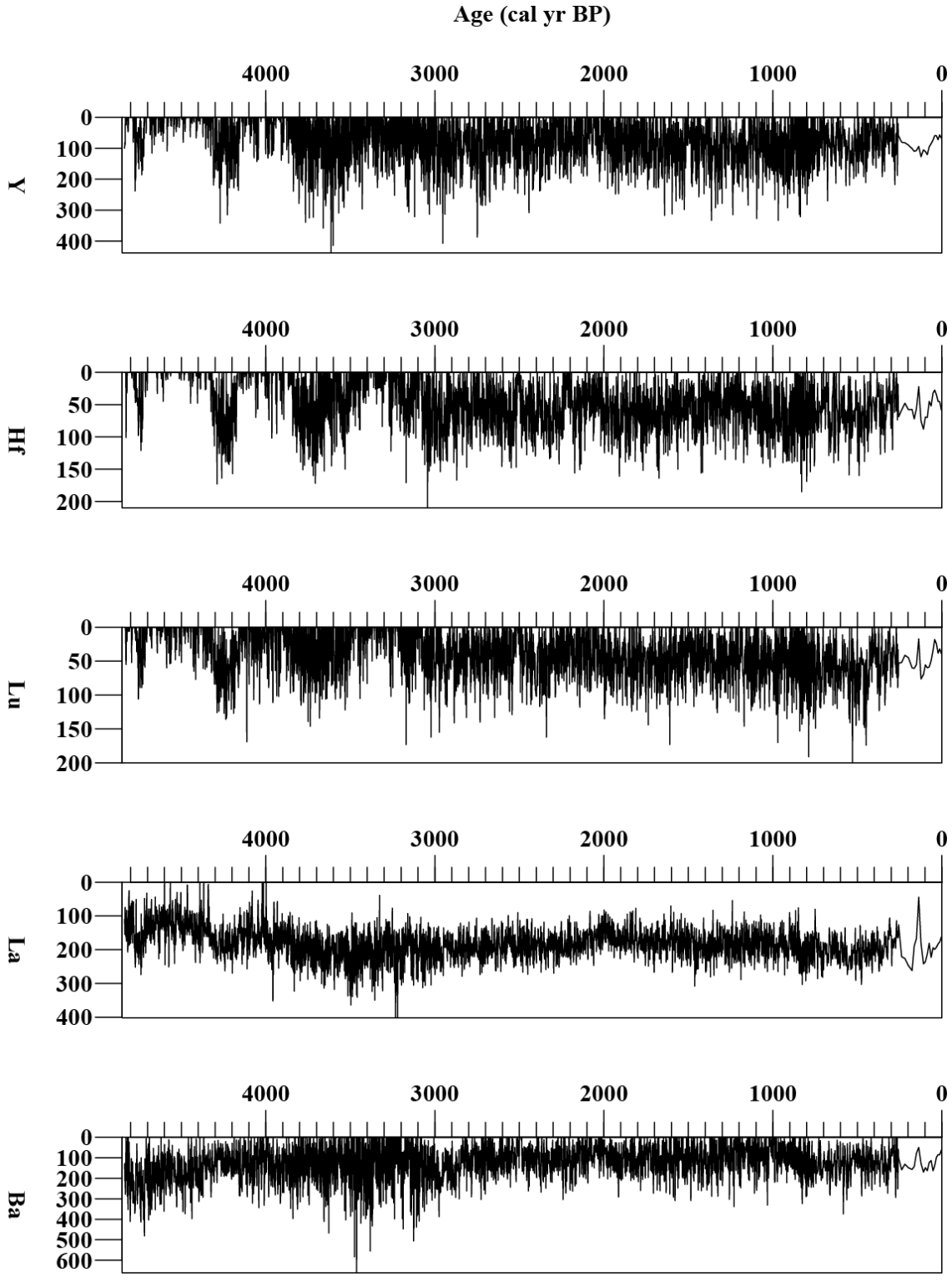
Age (cal yr BP)
4000
3000
2000
1000
0
Y
0
100
200
300
400
Hf
0
50
100
150
200
Lu
0
50
100
150
200
La
0
100
200
300
400
Ba
0
100
200
300
400
500
600

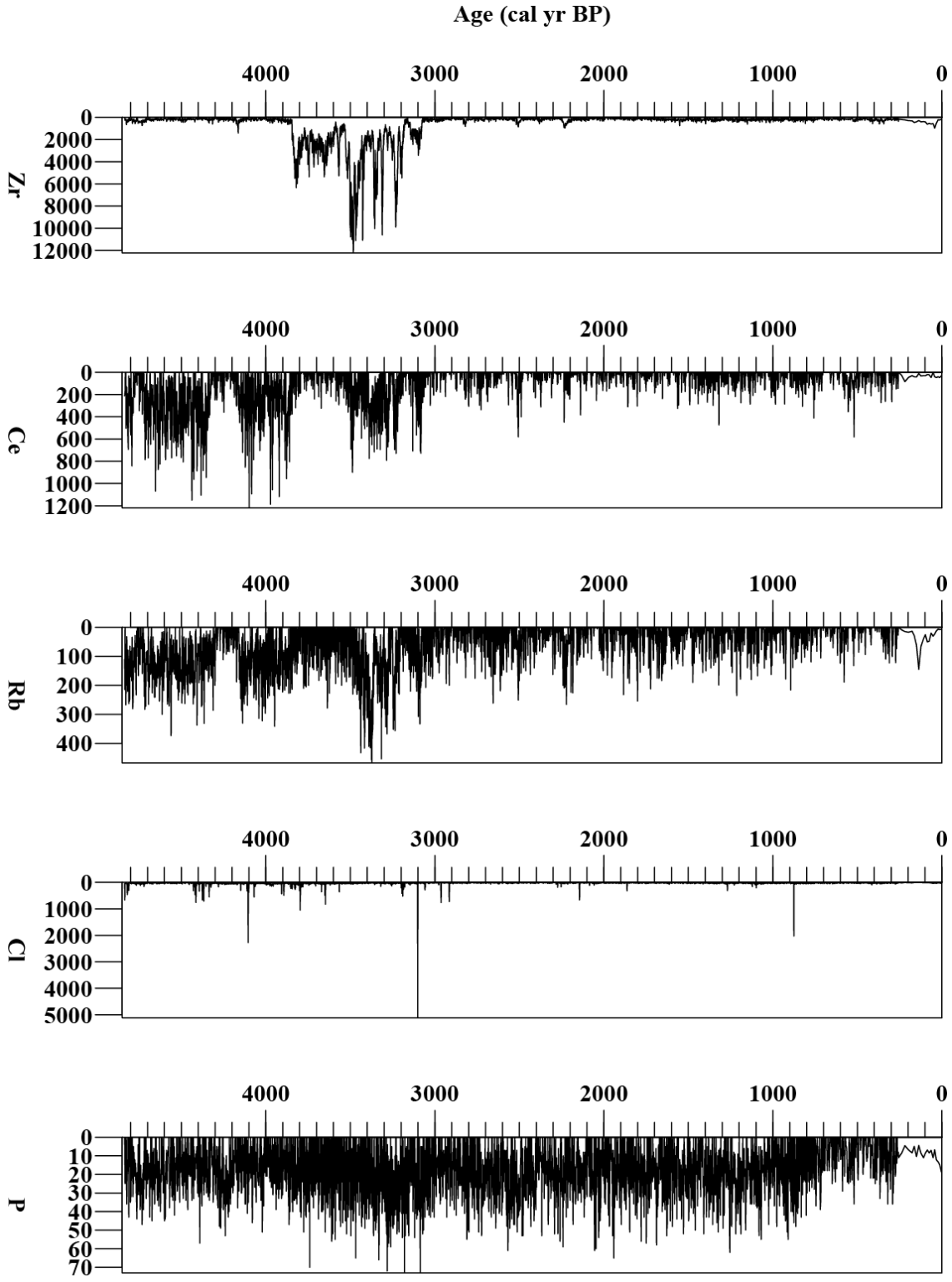
Age (cal yr BP)
4000
3000
2000
1000
0
Zr
0
2000
4000
6000
8000
10000
12000
Ce
0
200
400
600
800
1000
1200
Rb
0
100
200
300
400
Cl
0
1000
2000
3000
4000
5000
P
0
10
20
30
40
50
60
70

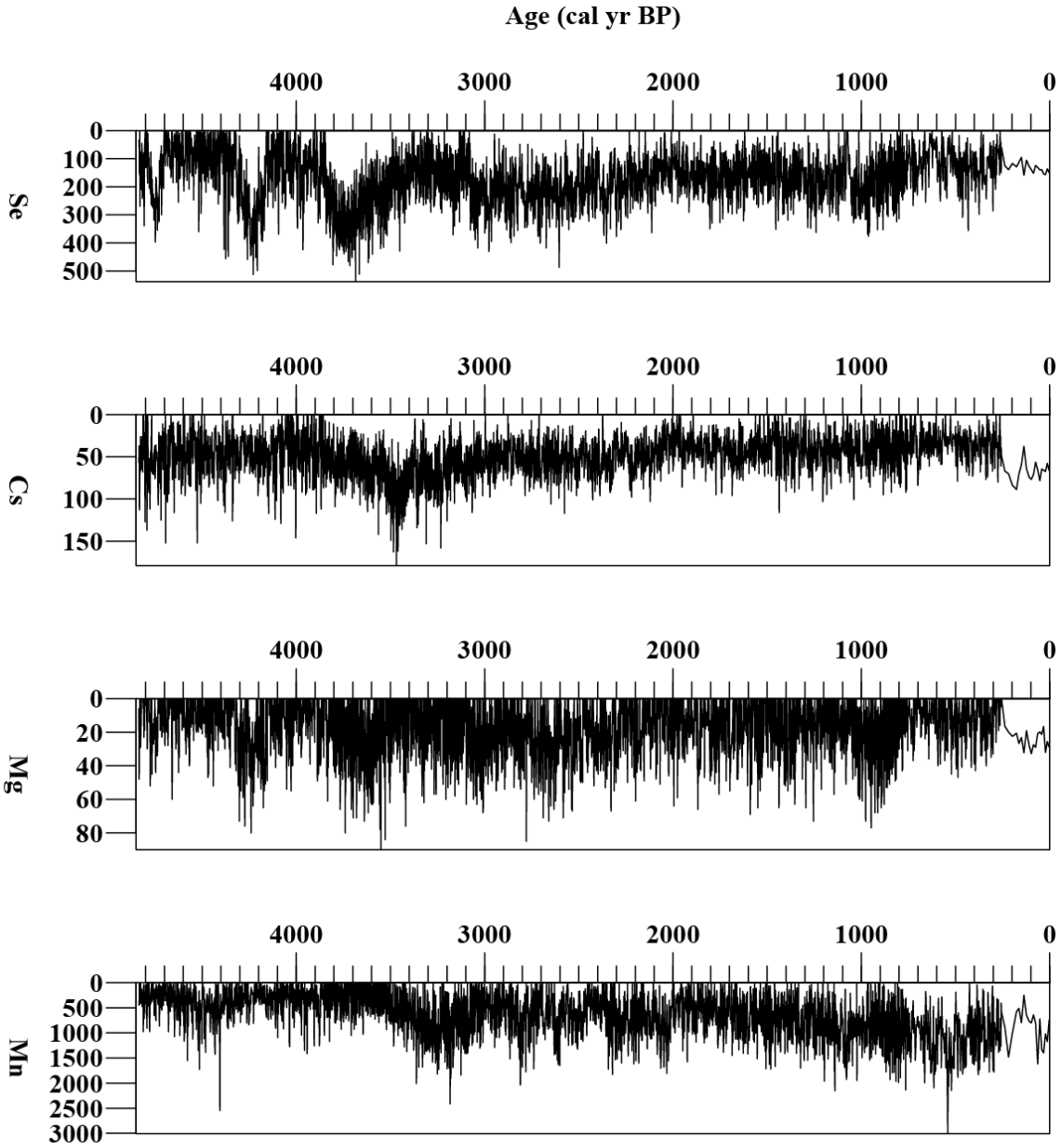
Age (cal yr BP)
4000
3000
2000
1000
0
Se
0
100
200
300
400
500
Cs
0
50
100
150
Mg
0
20
40
60
80
Mn
0
500
1000
1500
2000
2500
3000

APPENDIX C: CORE CORRELATION

Correlation of extruded core and drive 1 of DWL core using Fe/cps and magnetic susceptibility measurements

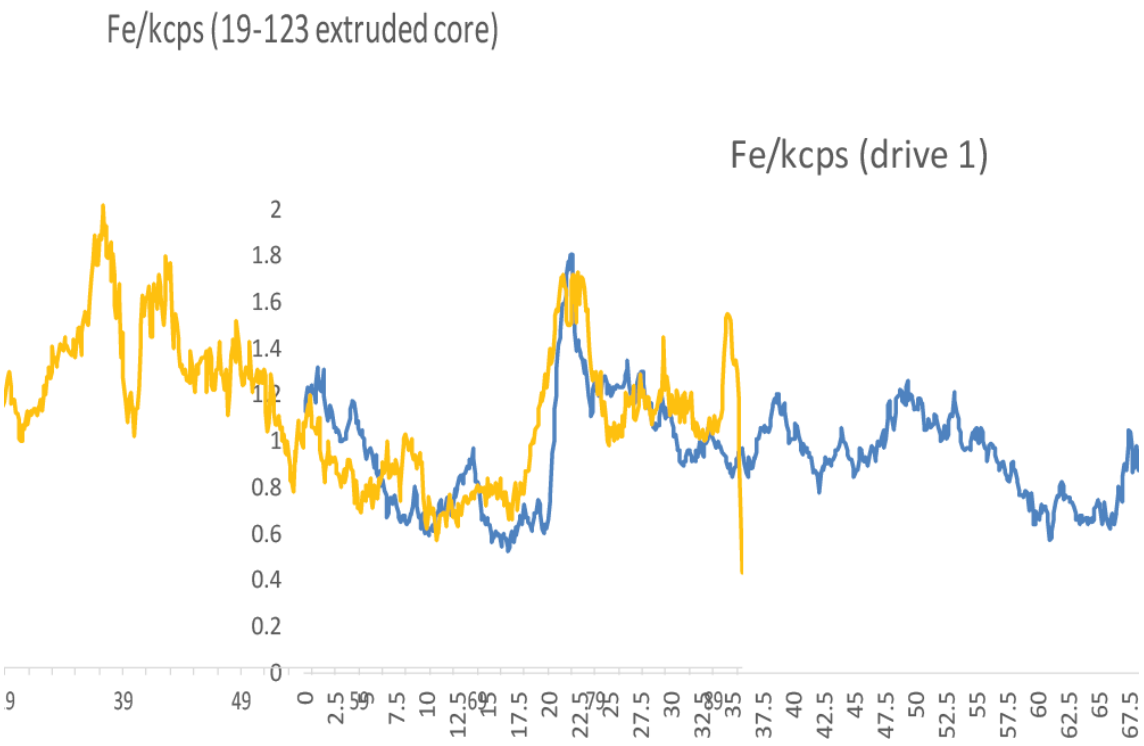

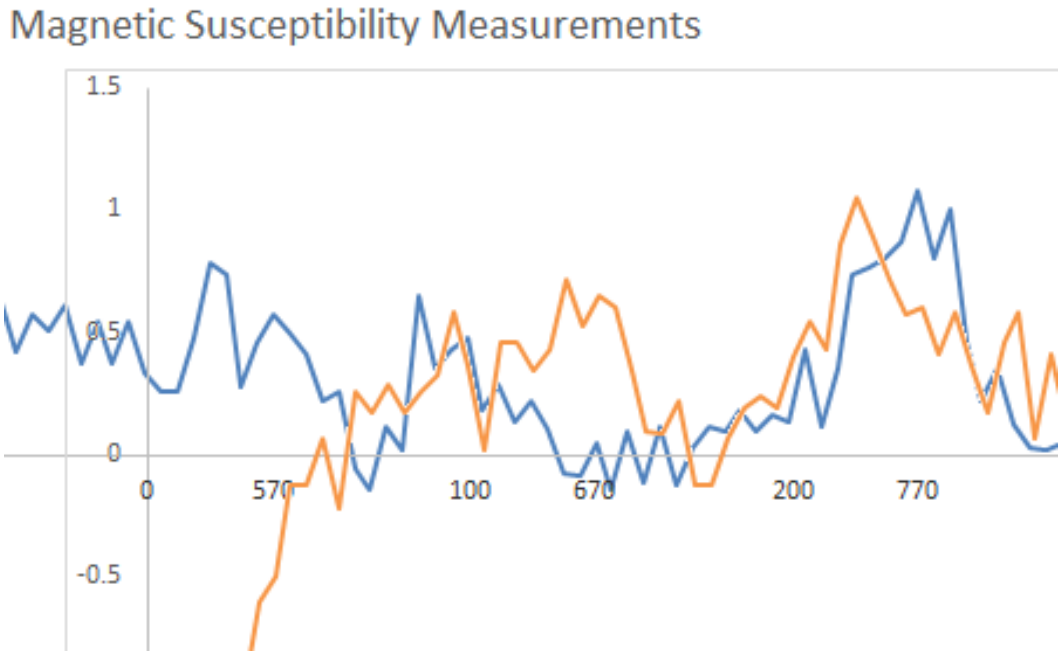

APPENDIX D: CARBON ISOTOPE AND C/N RATIO RAW DATA

Sample number	δ13C	%C	%N	C/N
DWL1	-31.3	15.7	0.9	18.0
2	-31.6	23.0	1.1	20.3
3	-31.3	22.8	1.1	21.2
4	-31.3	13.4	0.7	18.3
5	-31.6	15.6	0.7	22.9
6	-31.9	14.2	0.7	21.0
7	-31.5	12.8	0.7	19.1
8	-31.7	12.7	0.7	18.2
9	-32.0	11.6	0.7	15.5
10	-32.6	13.8	0.8	16.5
11	-30.8	8.2	0.5	15.8
12	-31.7	10.5	0.6	17.5
13	-29.8	7.0	0.4	17.0
14	-32.0	10.1	0.8	12.9
15	-31.6	11.8	0.6	19.8
16	-32.4	12.2	0.8	15.0
17	-26.9	3.5	0.1	34.3
18	-30.9	12.7	0.7	17.6
19	-28.7	3.0	0.1	25.8
20	-29.1	3.1	0.3	9.5
21	-28.0	4.3	0.5	9.3
22	-33.6	6.3	0.3	19.1
23	-29.0	35.2	5.1	6.9
24	-28.1	24.9	3.6	7.0
25	-28.7	14.3	1.7	8.6
26	-28.1	20.8	2.3	9.1
27	-28.2	0.7	0.0	29.9
28	-28.3	0.8	0.0	30.2
29	-28.3	1.9	0.5	3.6
30	too small	0.2	0.0	38.8
31	-28.2	0.5	0.0	42.8
32	-28.2	0.5	0.0	38.1
33	-27.7	0.2	0.0	32.5
34	-28.5	48.6	4.6	10.5
35	too small	0.1	0.0	26.3
36	-27.5	0.2	0.0	33.5
37	too small	0.0	0.0	22.5
38	too small	0.1	0.0	31.0
39	-27.4	3.5	0.1	28.5
40	too small	0.1	0.0	44.0